A comparative analysis of the vestibular apparatus in *Epipliopithecus vindobonensis*: Phylogenetic implications

Alessandro Urciuoli [a,*], Clément Zanolli [b], Amélie Beaudet [c,d], Marta Pina [a,e], Sergio Almécija [f,g,a], Salvador Moyà-Solà [a,h,i], David M. Alba [a,*]

[a] *Institut Català de Paleontologia Miquel Crusafont, Universitat Autònoma de Barcelona, Edifici ICTA-ICP, c/ Columnes s/n, Campus de la UAB, 08193 Cerdanyola del Vallès, Barcelona, Spain*

[b] *Univ. Bordeaux, CNRS, MCC, PACEA, UMR 5199, F-33600 Pessac, France*

[c] *School of Geography, Archaeology and Environmental Studies, University of the Witwatersrand, Private Bag 3, Johannesburg, WITS 2050, South Africa*

[d] *Department of Anatomy, University of Pretoria, PO Box 2034, Pretoria, 0001, South Africa*

[e] *School of Earth and Environmental Sciences, Faculty of Science and Engineering, University of Manchester, 176 Oxford Road, Manchester M13 9PL, UK*

[f] *Division of Anthropology, American Museum of Natural History, Central Park West at 79th Street, New York, NY 10024, USA*

[g] *New York Consortium in Evolutionary Primatology, New York, NY, USA*

[h] *Institució Catalana de Recerca i Estudis Avançats (ICREA), Passeig de Lluís Companys 23, 08010 Barcelona, Spain*

[i] *Unitat d'Antropologia (Departament de Biologia Animal, Biologia Vegetal i Ecologia), Universitat Autònoma de Barcelona, Campus de la UAB s/n, 08193 Cerdanyola del Vallès, Barcelona, Spain*

*Corresponding authors.

E-mail address: alessandro.urciuoli@icp.cat (A. Urciuoli); david.alba@icp.cat (D.M. Alba).

Acknowledgements

This research has been funded by the Agencia Estatal de Investigación (CGL2016-76431-P and CGL2017-82654-P, AEI/FEDER EU; and BES-2015-071318 to A.U.), the Generalitat de Catalunya (CERCA Programme, and consolidated research groups 2017 SGR 86 and 2017 SGR 116 GRC), the French Centre National de la Recherche Scientifique, the Leakey Foundation (research grant), and the Synthesys Project (AT-TAF-4689; http://synthesys3.myspecies.info/), which is financed by the European Community Research Infrastructure Action under the FP7. Part of the analyses were performed using High Performance Computing resources from BSC (BCV-2020-1-0008). We are grateful to Jose Torres for the technical help provided in the setup of the analysis. We thank the following people for providing or permitting access to CT scans: Ursula Göhlich (*Epipliopithecus* NHMW 1970/1397/0003), Martin Dockner, Loïc Costeur (*Epipliopithecus* NMBOE 303), Lorenzo Rook (*Oreopithecus*), José Braga (human specimens), Lynn Copes, Lynn Lucas, and the MCZ (part of the scans used in the study, funded by NSF DDIG #0925793 and Wenner-Gren Foundation Dissertation Grant #8102 to Lynn Copes), Richard Kay (*Homunculus* and *Dolichocebus*),Timothy Ryan (*Aegyptopithecus*; funded by NSF BCS-0416164 to Timothy Ryan and the Leakey Foundation), and the Division of Fossil Primates of the Duke Lemur Center (*Parapithecus*). We also thank Erik Seiffert and Steven Heritage for providing a digital rendering of *Parapithecus*. Finally, we thank the Editor (Andrea Taylor), the Associate Editor, and three anonymous reviewers for useful comments that helped us to improve a previous version of this paper.

A comparative analysis of the vestibular apparatus in *Epipliopithecus vindobonensis*: Phylogenetic implications

Abstract

Pliopithecoids are an extinct group of catarrhine primates from the Miocene of Eurasia. More than fifty years ago, they were linked to hylobatids due to some morphological similarities, but most subsequent studies have supported a stem catarrhine status, due to the retention of multiple plesiomorphic features (e.g., the ectotympanic morphology) relative to crown catarrhines. More recently, some morphological similarities to hominoids have been noted, raising the question of whether they could be stem members of this clade. To re-evaluate these competing hypotheses, we examine the morphology of the semicircular canals of the bony labyrinth of the middle Miocene pliopithecid *Epipliopithecus vindobonensis*. The semicircular canals are suitable to test between these hypotheses because: (1) they have been shown to embed strong phylogenetic signal and reliably discriminate among major clades; (2) several potential hominoid synapomorphies have been identified previously in the semicircular canals; and (3) semicircular canal morphology has not been previously described for any pliopithecoid. We use a deformation-based (landmark-free) three-dimensional geometric morphometric approach to compare *Epipliopithecus* with a broad primate sample of extant and extinct anthropoids. We quantify similarities in semicircular canal morphology using multivariate analyses, reconstruct ancestral morphotypes by means of a phylomorphospace approach, and identify catarrhine and hominoid synapomorphies based on discrete characters. *Epipliopithecus* semicircular canal morphology most closely resembles that of platyrrhines and *Aegyptopithecus* due to the retention of multiple anthropoid symplesiomorphies. However, *Epipliopithecus* is most parsimoniously interpreted as a stem catarrhine more derived than *Aegyptopithecus* due to the possession of a crown catarrhine synapomorphy

(i.e., the rounded anterior canal), combined with the lack of other catarrhine and any hominoid synapomorphies. Some similarities with hylobatids and atelids are interpreted as homoplasies likely related to positional behavior. The semicircular canal morphology of *Epipliopithecus* thus supports the common view that pliopithecoids are stem catarrhines.

Keywords: Pliopithecidae; Catarrhini; Miocene; Inner ear; Phylogeny; Geometric morphometrics

1. Introduction

1.1. The phylogenetic position of pliopithecoids

Pliopithecoids are an extinct superfamily of catarrhine primates, recorded in Eurasia from the early to the late Miocene (Andrews et al., 1996; Begun, 2002, 2017; Harrison, 2005, 2013). Their first occurrence, in the early Miocene of China (~18–17 Ma; Harrison and Gu, 1999; Begun, 2002; Harrison, 2013), slightly predates the oldest record of large-bodied apes in Eurasia (Heizmann and Begun, 2001; Casanovas-Vilar et al., 2011). In the absence of older (earliest Miocene) catarrhines in that continent, pliopithecoids are assumed to have an African origin (Harrison, 1987, 2013; Begun, 2017). Like apes, pliopithecoid ancestors probably dispersed into Eurasia before the Langhian transgression, which was possible due to the lowered sea level and tectonic events that led to the closure of the Tethys Seaway and the establishment of an intermittent terrestrial corridor beginning at ~19 Ma (Harzhauser et al., 2007; Harrison, 2013).

Decades ago, pliopithecoids were considered to be phylogenetically related to hylobatids due to some superficial resemblances in cranial morphology as well as body size and proportions (e.g., Hürzeler, 1954; Zapfe, 1958, 1960, 1961; Simons and Fleagle, 1973). Currently, they are generally considered a clade of stem catarrhines—as supported by the retention of several cranial and postcranial features that are plesiomorphic

compared to the crown members of the group (Andrews, 1975; Ciochon and Corruccini, 1977; Fleagle, 1984; Harrison, 1987, 2005, 2013; Andrews et al., 1996; Begun, 2002, 2017). The divergence of pliopithecoids before the split of crown catarrhines is further supported by most recent cladistic analyses (Zalmout et al., 2010; Stevens et al., 2013; Nengo et al., 2017; Gilbert et al., 2020), implying a long ghost lineage of ca. 12–14 Myr for pliopithecoids (Begun, 2017). The exception is the cladistic analysis by Alba et al. (2015), which recovered pliopithecoids as a clade of stem hominoids—thereby eliminating the need to hypothesize a long gap in the pliopithecoid fossil record. Most recently, Almécija et al. (2019) further documented similarities in femoral morphology between pliopithecoids (*Epipliopithecus*) and extant hominoids, thereby casting additional doubts on the status of pliopithecoids as stem catarrhines. Further uncertainty in this regard stems from the fact that no tail vertebrae are known from pliopithecoids (Begun, 2017). Based on sacral morphology, Zapfe (1958, 1961) argued that no external tail would have been present, as in hominoids; although this has subsequently been rebutted (Ankel, 1965; Russo, 2016), available evidence in this regard remains uncertain.

There are multiple genera of pliopithecids (Harrison and Gu, 1999; Moyà-Solà et al., 2001; Begun, 2002, 2017; Harrison, 2005, 2013; Alba et al., 2010; Alba and Moyà-Solà, 2012; Alba and Berning, 2013; Sankhyan et al., 2017; Harrison et al., 2020), which, following Harrison et al. (2020), we provisionally group into four different families: dionysopithecids (*Dionysopithecus* and *Platodontopithecus*), krishnapithecids (*Krishnapithecus*), pliopithecids (*Pliopithecus* and *Epipliopithecus*), and crouzeliids (*Plesiopliopithecus*, *Barberapithecus*, *Anapithecus*, *Egarapithecus*, and *Laccopithecus*). However, it is noteworthy that the treatment of these genera at the family rank, and even the placing of some genera in one or another group, differs among authors (e.g., compare Alba and Moyà-Solà, 2012 with Begun, 2017). Such disagreements largely stem from the

fact that the internal phylogeny of pliopithecoids is still unclear and that their affinities with fossil catarrhines from Africa remain uncertain (e.g., Harrison, 2013).

1.2. Evidence from Epipliopithecus

Deciphering the phylogenetic relationships of most pliopithecoids is hampered by the fact that they are mostly known by fragmentary dentognathic remains, with the exception of *Epipliopithecus vindobonensis*, whose craniodental and postcranial morphology is well documented by several skeletons from the middle Miocene (MN6, ~14.85–13.45 Ma[1]) karstic infillings of Devínska Nová Ves, Slovakia (Zapfe, 1958, 1961; Andrews et al., 1996; Begun, 2002; Harrison, 2013). *Epipliopithecus* was originally established as a subgenus of *Pliopithecus* by Zapfe and Hürzeler (1957), being subsequently considered a junior subjective synonym of the latter (e.g., Andrews et al., 1996; Harrison and Gu, 1999; Moyà-Solà et al., 2001; Harrison, 2005, 2013; Alba et al., 2010) or a distinct genus (e.g., Begun, 2002; Alba and Moyà-Solà, 2012; Arias-Martorell et al., 2015; Alba et al., 2015; this study). From a locomotor viewpoint, *E. vindobonensis* has been variously depicted as an arboreal or semiterrestrial generalized quadruped with varying degrees of climbing and suspensory abilities (see discussion in Arias-Martorell et al., 2015). From a phylogenetic perspective, its purported stem catarrhine status has been supported by features such as the short and only partially enclosed ectotympanic, the presence of entepicondylar foramen in the distal humerus, and single hinge-like carpometacarpal joint in the thumb (Zapfe, 1961; Szalay and Delson, 1979; Harrison, 1987, 2005; Andrews et al., 1996; Begun, 2002, 2017).

[1] Age uncertainly based on the boundaries recognized for MN6 (van der Meulen et al., 2011).

The external morphology of the petrosal bone of *E. vindobonensis* (Zapfe, 1961; Szalay, 1975; Fricano, 2018) has been of utmost significance in the discussion of its phylogenetic affinities, given that the presence of a tubular ectotympanic is considered synapomorphic of crown catarrhines (e.g., Szalay, 1975; Szalay and Delson, 1979; Harrison, 1987, 2005; Andrews et al., 1996; Begun, 2002; Zalmout et al., 2010; Alba et al., 2015; Nengo et al., 2017). The possibility remains that such ossification took place to some extent independently in cercopithecoids, hominoids and/or other anthropoids such as pliopithecoids (Begun, 2002, 2017; Alba et al., 2015). However, other features of *Epipliopithecus* also appear plesiomorphic as compared to crown catarrhines and show no particular similarities with hominoids, namely: the large postglenoid process separated from the acoustic meatus, as in platyrrhines (Zapfe, 1961); the lack of ossification in the tentorium cerebelli (unlike in most platyrrhines and stem anthropoids, but similar to *Aegyptopithecus* and crown catarrhines; Kay et al., 2009a); and the deep subarcuate fossa (Zapfe, 1961), as in platyrrhines and most anthropoids except hominids (Gannon et al., 1988; Kunimatsu et al., 2019). In contrast, the inner ear morphology of *Epipliopithecus* has not been described and therefore its potential phylogenetic implications remain unexplored.

1.3. The bony labyrinth of the inner ear

Among the inner cavities of the petrosal, the bony labyrinth of the inner ear is constituted by the semicircular canals (SCs) and the vestibule (which together host the soft-tissue structures linked with the sense of balance) plus the cochlea. Semicircular canal size (e.g., Spoor et al., 2007; Silcox et al., 2009; Ryan et al., 2012; Grohé et al., 2018) and orientation (David et al., 2010; Malinzak et al., 2012; Berlin et al., 2013; Perier et al., 2016; Gonzales et al., 2019) have been frequently used for inferring agility, while the shape of the canals as a whole has tentatively been linked to positional behavior (Le

126 Maître et al., 2017). At the same time, recent studies have demonstrated that the SCs bear
127 strong phylogenetic signal among anthropoids (Lebrun, 2010, 2012; Urciuoli et al., 2019,
128 2020; del Rio et al., 2020; Morimoto et al., 2020) and other mammals (e.g., Grohé et al.,
129 2015; Mennecart et al., 2016, 2017; Costeur et al., 2018).

130 Although adaptively relevant characters may constitute synapomorphies of
131 particular clades, arguably their relationship with function makes them potentially more
132 prone to homoplasy. However, the correlation between SC morphology and positional
133 behavior has recently been questioned by some studies (i.e., Rae et al., 2016; del Río et
134 al., 2020; Morimoto, et al., 2020), and SC shape variation has been shown to largely follow
135 the expectations of a Brownian motion mode of evolution in both platyrrhines (del Río et
136 al., 2020) and catarrhines (Urciuoli et al., 2020). These results are in accordance with
137 those obtained for the bony labyrinth as a whole, showing that its morphology reflects
138 phylogenetic relatedness as inferred from molecular data (Lebrun et al., 2010; Ekdale,
139 2013; Macrini, et al., 2013; Billet et al., 2015). Cumulatively, this evidence suggests that
140 bony labyrinth morphology is phylogenetically informative among mammals (Mennecart et
141 al., 2017) and may thus potentially illuminate the phylogenetic relationships of extinct
142 primates. Following Mennecart and Costeur (2016), who suggested that inner ear
143 structures might be highly informative for large cladistics analyses, Urciuoli et al. (2020)
144 explored catarrhine SC shape variation among catarrhines and proposed several potential
145 synapomorphies for crown hominoids.

146 Here we test between two different phylogenetic hypotheses for *Epipliopithecus*,
147 one hypothesis being that *Epipliopithecus* is a stem catarrhine, the other hypothesis that
148 *Epipliopithecus* is a hominoid, based on the information provided by the shape of the SCs
149 and vestibule. This morphology is described here for the first time using a three-
150 dimensional geometric morphometric (3DGM) approach applied to a broad sample of
151 extant and fossil anthropoids (Urciuoli et al., 2020). We refrained from analyzing the entire

bony labyrinth (i.e., including also the cochlea) because its potential for phylogenetic reconstruction among primates is currently unclear. A recent analysis in platyrrhines suggested that cochlear shape departs from a Brownian motion mode of evolution (Blomberg's K < 1; del Río et al., 2020), thus potentially reflecting a greater influence of function (and likely homoplasy due to similar selection pressures) than is the case for the SCs and vestibule. This is in agreement with previous studies linking several macroscopic cochlear features to hearing capabilities (e.g., Manoussaki et al., 2006; Kirk and Gosselin-Ildari, 2009; Coleman and Colbert, 2010). More detailed morphometric analyses of this structure among anthropoids is thus required to determine whether cochlear morphology can be meaningfully used to decipher the phylogenetic relationships of extinct catarrhines such as *Epipliopithecus*.

2. Materials and methods

2.1. Described material

We inspected three petrosals of *E. vindobonensis* belonging to two individuals from Devínska Nová Ves, Slovakia (Zapfe, 1960, 1961): NMB OE 303a, b (individual III), left (a) and right (b), housed in the Naturhistorisches Museum of Basel, Switzerland[2]; and NHMW 1970/1397/0003 (individual II), right, housed in the Naturhistorisches Museum of Wien, Austria.

2.2. Comparative sample

The comparative sample includes µCT scans of 162 dried crania and temporal bones belonging to 31 extant anthropoid species (see Supplementary Online Material [SOM] Table S1 for the sample size of the extant species), plus five fossil anthropoids

[2] Morimoto et al. (2020) included the bony labyrinth of NMB OE 303a in their comparative study but did not depict or specifically describe its morphology.

(SOM Table S2): the stem anthropoid *Parapithecus* (Bush et al., 2004), the stem catarrhine *Aegyptopithecus* (Simons et al., 2007), the stem platyrrhines *Dolichocebus* (Kay et al., 2009b) and *Homunculus* (Fulwood et al., 2016), and the hominoid *Oreopithecus* (Rook et al., 2004).

2.3. *Sample preparation*

NMB OE 303 was scanned with a Phoenix Nanotom®, GE at the Biomaterials Science Centre of the University of Basel (Switzerland) obtaining a voxel size of 25 µm. NHMW 1970/1397/0003 was scanned at the Vienna µCT-Lab using a Viscom X8060 (Viscom XT9190-THP X-ray tube) obtaining a voxel size of 22 µm. The canals and vestibule of NMB OE 303a, b were filled with air, while in NHMW 1970/1397/0003 they were partially filled with sediment. In both cases we segmented the SCs and vestibule cavities using the 'watershed' tool of Avizo v. 9.0.1 (FEI Visualization Sciences Group, Houston), with additional manual corrections for NHMW 1970/1397/0003. The 3D surfaces of NMB OE 303b and NHMW 1970/1397/0003 were mirrored for comparison. The 3D meshes of the two individuals are available from MorphoSource (see Table 1).

The µCT scans of most extant comparative species and of fossil anthropoids were accessed from MorphoSource.org digital repository (https://www.morphosource.org) with the exception of *Oreopithecus bambolii* petrosal, which was kindly provided by Lorenzo Rook (see SOM Table S2 for voxel sizes). Further details about the µCT scans of the extant comparative sample (voxel sizes, exact source, DOI, etc.) can be found in Urciuoli et al. (2020: Supplementary File 1). The slice stacks of these crania were processed using Avizo v. 9.0.1. and the left bony labyrinth was segmented using the semiautomatic 'watershed' tool of Avizo (with additional manual corrections in the case of partially filled canals found in the fossil specimens) and digitally extracted; when the left bony labyrinth was unavailable, the right one was mirrored. As in Urciuoli et al. (2020), the SCs and the

vestibule were separated from the cochlea by cutting the generated 3D meshes immediately inferior to the saccule and the oval window, using landmarks placed along the maximum curvature of the junction between the vestibule and the cochlea as reference for the cutting plane (Fig. 1). The resulting holes were filled with a flat surface using Geomagic Studio v. 2014.3.0 (3D Systems, Rock Hill, USA). Prior to the 3DGM analysis, the surfaces were first roughly prealigned by manually superimposing the meshes to ensure biological correspondence. Subsequently, the alignment was automatically refined using the Avizo module 'Align Surface' with the 'rigid + uniform' option. Similar to Procrustes superimposition, this module minimizes the distances between the faces of each surface by scaling, translating and rotating the analyzed meshes. The phylogenetic relationships of the extinct taxa included in the analyses, relative to extant anthropoids, are summarized in Figure 2.

2.4. Shape analysis

Differences in vestibule and SC shape were evaluated using a landmark-free 3DGM technique based on deformation, which relies on the geometrical correspondence of continuous surfaces and computes the magnitude and direction of deformation of the analyzed meshes from a group-average template (Glaunès and Joshi, 2006; Durrleman et al., 2012a, b; Dumoncel et al., 2014; Beaudet et al., 2016; Urciuoli et al., 2020). The deformations are mathematically modeled to obtain a one-to-one correspondence of the 3D space using the open-source software Deformetrica 4 (Bône et al., 2018). This technique yields results similar to landmark-based 3DGM methods while more easily tracking changes in volume (Urciuoli et al., 2020), and is less prone to biases introduced by the design of landmarking protocols, caused by the inherent difficulty to adequately capture complex 3D shapes based on a reduced number of homologous landmarks.

Due to the high computational power required, the sets of vectors, representing the flow of deformations from the initial position of the control points on the template to the target shape, were computed in the Barcelona Supercomputing Center (BSC) using the MinoTauro cluster (https://www.bsc.es/marenostrum/minotauro). To identify major patterns of shape variation across the sample, the resulting sets of vectors were inspected using between-group principal component analysis (bgPCA; Mitteroecker and Bookstein, 2011), using major clades (platyrrhines, cercopithecoids, hylobatids, and hominids) as the grouping factor (Urciuoli et al., 2020). To address recent concerns about the use of bgPCA based on highly multivariate data sets, such as those generated by 3DGM, and to rule out the presence of spurious groupings in our results (Bookstein, 2019; Cardini, et al., 2019), we computed cross-validated bgPCA scores. These were obtained by iteratively repeating the bgPCA on a subset of the sample. The cross-validated bgPCA scores were then compared to those obtained with standard bgPCA (Cardini and Polly, 2020). The affinities of fossil specimens with the groups defined a priori in the bgPCA were evaluated using the 'typprobClass' function of the Morpho package v. 2.7 (Schlager, 2017) in R v. 3.6.1 (R Core Team, 2019). This function computes posterior probabilities of group membership based on the Mahalanobis distances between the bgPC scores of fossil specimens and group centroids. Null hypotheses of group membership were rejected at $p < 0.05$. Similarities among anthropoid species were also evaluated by running a cluster analysis (Ward's method) on the Mahalanobis distances between pairs of bgPCA species centroid scores using the 'ward.D2' method of the 'hclust' function of the 'stats' package in R. The cophenetic correlation coefficient, which allows one to evaluate how faithfully the obtained dendrogram preserves the pairwise distances between the original unmodeled datapoints, was calculated using the same package.

In addition, we inspected the volumetric proportions of *Epipliopithecus* and the remaining fossil taxa included in the analysis, and determined the correlation between log-

transformed cube root canal volume (ln VolSC, mm) and log-transformed canal length (ln L, mm) by means of ordinary least-squares regression. Given that previous analyses identified an allometric grade shift between hominids and nonhominid anthropoids (Urciuoli et al., 2020), separate regression lines were computed for hominids and nonhominid anthropoid taxa using the 'stats' package in R.

2.5. Phylomorphospace, ancestral state estimation, and phylogenetic signal

To intuitively visualize the direction and magnitude of evolutionary change we relied on a phylomorphospace approach (Sidlauskas, 2008), by which a phylogenetic tree is projected onto the tangent space defined by the bgPCA of our shape data. Ancestral states for the internal nodes are estimated using a maximum likelihood method for continuous characters via the 'fastAnc' function of the 'phytools' version 0.6-60 package for R (Revell, 2012), while the tips of the tree branches correspond to the centroid scores for the included taxa. We repeated the analyses using two composite phylogenetic trees, one with *Epipliopithecus* as a stem catarrhine and the other with this taxon as a stem hominoid (Figs. 2 and 3). For extant taxa we relied on a Bayesian phylogenetic analysis of eleven mitochondrial and six autosomal genes downloaded from the 10kTrees Website v. 3 (Arnold et al., 2010). Extinct species were added based on their phylogenetic position, their divergence being arbitrarily placed 1 Myr before the estimated divergence age of the next derived node, and tip ages based on their chronostratigraphic age. We used the following tip age estimates: *Epipliopithecus* 14.15 Ma (mean of 14.85 and 13.45 Ma, the maximum-minimum age range for MN6 in central Europe according to van der Meulen et al., 2011); *Aegyptopithecus* and *Parapithecus*, 29.85 Ma (mean of 30.2 and 29.5 Ma, based on the revised age range of the fauna of quarries I and M of the Jebel Qatrani Formation of the Fayum depression by Seiffert, 2006); *Dolichocebus*, 20.5 Ma (mean of 21.0 and 20.0 Ma age provided by Kay, 2015); *Homunculus*, 17.2 Ma (mean of 17.9 and

16.5 Ma age provided by Kay, 2015); and *Oreopithecus* 6.75 Ma (mean of 7.0 and 6.5 Ma for the last occurrence according to Rook et al., 2000).

The phylogenetic signal embedded in the shape data was measured using Pagel's λ (Pagel, 1999) and Blomberg's K (Blomberg et al., 2003), together with the multivariate version of Blomberg's K (K_{mult}; Adams, 2014). Pagel's λ and Blomberg's K were computed using the 'phylosig' function of the 'phytools' package in R, while K_{mult} was computed with the 'physignal' function of the 'geomorph' package v. 3.1.0 in R (Adams et al., 2019). These metrics were computed based on extant taxa only (Arnold et al., 2010).

Ancestral node morphologies were computed from the bgPC scores for the last common ancestors (LCAs) estimated by means of maximum likelihood, which were rotated and translated from the morphospace back into the deformation field space, generating a set of momentum vectors that were used in Deformetrica 4 to warp the template surface into the target LCA morphology. Volumetric proportions for the LCAs were computed based on the rescaled 3D models obtained from the phylomorphospace approach; the scaling factor for each LCA was estimated using the 'anc.ML' function of the R package 'phytools'. Morphological similarities between *Epipliopithecus* and the LCA centroids were assessed by means Euclidean distances between the *Epipliopithecus* centroid and the LCA bgPC scores, weighted on the basis of the percentage of variance explained by each bgPC and computed using the 'distances' function of the 'distances' package version 0.1.8 in R (Savje, 2019).

The two phylogenetic hypotheses for *Epipliopithecus* depicted in Figure 3 were assessed further based on the coding of seven discrete characters that were deemed of phylogenetic significance based on shape comparisons and analyses. The resulting character-taxon matrix was analyzed for character congruence against a fixed topology consistent with the phylogenetic hypotheses depicted in Figure 3. For both cladograms, three indices customarily employed in cladistics (Farris, 1989) were computed in PAUP* v.

4.0a168 for Mac (Swofford, 2003) to assess the most parsimonious hypothesis: the consistency index (CI), the retention index (RI), and the rescaled consistency index (RC).

3. Results

3.1. Description and comparisons

The three bony labyrinths of *E. vindobonensis* are well preserved—except for the lateral canal of NMB OE 303b, which shows a small fracture in the bony encasing—and are not affected by diagenetic deformation, thereby permitting a straightforward extraction of the 3D surfaces of the vestibular apparatus bony labyrinth (Fig. 4a–c). Overall, the canals are fairly slender, as in platyrrhines and cercopithecins, falling within their variability as shown by a bivariate plot of SC volume vs. length (Fig. 5; Table 2; SOM Table S3). The bony vestibule is large, albeit less so than in hominids. The anterior and posterior canals are larger than the lateral canal, as in platyrrhines (Fig. 4e–i) and modern humans (Fig. 4u).

The *E. vindobonensis* common crus (CC) is long, as in extant platyrrhines (Fig. 4g–i) and in *Dolichocebus* (Fig. 4e), but unlike in most catarrhines. The trajectories of the anterior and posterior canal form a right angle when merging at the CC apex. Despite some similarities, the morphology of *Epipliopithecus* is clearly distinguishable from that of *Dolichocebus* and *Parapithecus* (Fig. 4d), as the CC is not posteromedially inclined and the anterior canal connection is placed more laterally.

The anterior canal of *E. vindobonensis* is slightly wider than tall (as in *Hoolock*; Fig. 4q), yet clearly rounded and lacking the vertical compression characteristic of extant hominoids (Fig. 4o–u), the anterosuperior elongation typical of hylobatids and *Pongo* (Fig. 4o–r; Urciuoli et al., 2020), and the extreme superior projection found in *Ateles* (Fig. 4g). The anterior canal of *Epipliopithecus* further differs from that of the stem anthropoid *Parapithecus* (Fig. 4d), the stem platyrrhine *Dolichocebus* (Fig. 4e), and the stem

catarrhine *Aegyptopithecus* (Fig. 4j), characterized by an almost triangular morphology (albeit less so in the last genus). The superiormost portion of the anterior canal bends medially, causing a moderate torsion of the canal trajectory. This morphology is also found in the stem platyrrhine *Homunculus* (Fig. 4f) and, to a lesser extent, *Chlorocebus* (Fig. 4l) and *Dolichocebus* (Fig. 4e), while in most cercopithecoids it is much more bent (e.g., *Macaca*; Fig. 4m). A sinuous trajectory of the anterior canal, although with a different morphology, is also displayed by other taxa (e.g., *Cebus*; Fig. 4i) and thus is not very informative from a phylogenetic viewpoint. Despite the aforementioned similarities, *Epipliopithecus* differs from the stem platyrrhines *Homunculus* (Fig. 4f) and *Dolichocebus* (Fig. 4e), from most extant platyrrhines (particularly *Ateles*; Fig. 4g), and from the stem catarrhine *Aegyptopithecus* (Fig. 4j), in displaying a much less mediolaterally compressed anterior canal.

The posterior canal of *Epipliopithecus* is slightly taller than wide, similar to that of *Alouatta* (Fig. 4h) and *Symphalangus* (Fig. 4p), but differs from the latter by displaying a less arched connection with the CC. The orientation of the posterior canal relative to the plane defined by the anterior canal is different in the two individuals of *Epipliopithecus*: it forms an obtuse angle in NHMW 1970/1397/0003 (resembling the hylobatid condition), but forms a right angle in NMB OE 303 (as in other anthropoids; SOM Fig. S2).

The lateral canal is rounded and smaller than the other canals (more so in NMB OE 303), as in stem platyrrhines (Fig. 4e, f) and the stem catarrhine *Aegyptopithecus* (Fig. 4j), although in *Epipliopithecus* this canal is not strongly compressed mediolaterally as in the latter taxon (Fig. 4j). The trajectory of the ampullary portion of the lateral canal slightly bends superiorly (more so in NMB OE 303; Fig. 4b, c), while the insertion of its slender part is located anteriorly to the base of the CC (particularly in NHMW 1970/1397/0003; Fig. 4a), so that—as in extant hominoids but unlike cercopithecoids—the lateral canal does not intersect the plane defined by the posterior canal. The lateral canal also shows a wave-like

shape, with its lateral-most tip pointing downwards, superficially resembling some individuals of *Pongo* (Fig. 4r), while differing from the morphology of *Trachypithecus* (Fig. 4k) and *Macaca* (Fig. 4m), where the canal bends inferiorly right before the ampullary portion.

3.2. Shape analysis

The bgPCA discriminates major anthropoid clades with just minimal overlap when the three axes are considered simultaneously (Fig. 6), thus closely resembling the previous results by Urciuoli et al. (2020) despite the increased number of platyrrhine taxa included here. The bgPCA results reported in Figure 6 closely resemble those derived using a cross-validated bgPCA (SOM Fig. S1), indicating that group separation is not spurious (Cardini and Polly, 2020).

The first principal component (bgPC1, which explains 59% of the variance) mainly reflects differences in volumetric proportions among the SCs and the volume they occupy relative to that of the bony vestibule, separating hominids (stout canals; quite negative scores) from both cercopithecoids and hylobatids (slender canals; positive to slightly negative scores), while platyrrhines (including stem taxa), the stem anthropoid *Parapithecus*, the stem catarrhine *Aegyptopithecus*, the stem hominoid *Oreopithecus*, and *Epipliopithecus* occupy an intermediate position in the morphospace. In particular, the two *Epipliopithecus* individuals, due to their fairly slender canals (Fig.4a–c), display similar intermediate scores along this axis, overlapping extensively with both extant and extinct platyrrhines in the overlap zone of cercopithecoids and hominoids (Fig. 6a, c).

In turn, bgPC2 (which explains 30% of the variance) accounts for differences in the size and shape of the anterior and posterior canals (Fig. 6a, d), in the position of the lateral canal ampullary insertion on the vestibule, and in CC length, separating most platyrrhines (positive scores) from catarrhines (moderately positive to negative scores). In particular,

platyrrhines possess large and very superiorly elongated canals in the portion close to the CC apex, as well as a flat lateral canal, which also connects more inferiorly on the vestibule with its ampullary portion. Catarrhines are more variable in these features, showing rounded to vertically compressed anterior and posterior canals, a shorter CC, and a variably sinuous lateral canal with its ampullary portion connecting more superiorly. *Epipliopithecus* displays moderately positive scores, falling within the range of several extant platyrrhines (*Aotus*, *Alouatta*, *Callithrix* and *Callicebus*), due to their large anterior and posterior canals, coupled with a long CC and a small lateral canal. Both the stem platyrrhines and *Oreopithecus* show similar moderately positive scores, while *Aegyptopithecus* and *Parapithecus* show markedly positive values due to their superiorly elongated vertical canals (Fig. 6a).

Finally, bgPC3 (which explains 11% of the variance) is driven by the position of the lateral canal relative to the posterior one, by the size and orientation of the posterior canal, as well as the shape of the anterior canal and CC thickness (Fig. 6b, e), separating hylobatids (most positive values) from most extant and fossil anthropoids (intermediate to negative scores). Hylobatids have a much larger gap between the lateral and posterior canals than other anthropoids except some modern humans, and their posterior canal is also smaller than, and forms an obtuse angle with, the large and anteriorly-protruding anterior canal. In contrast, in most cercopithecoids, *Aotus*, and *Callithrix,* the lateral canal broadly intersects with the posterior canal, while in the African great apes, *Theropithecus*, and *Cebus* the canals are only minimally separated. In addition, in all extant anthropoids except hylobatids, the plane of the posterior canal forms a right angle with the anterior canal, which does not project anteriorly. Both *Epipliopithecus* individuals display positive scores (NMB OE 303 with lower values), overlapping with some hylobatids (mainly *Hoolock*) and other extant anthropoids (particularly the hominids *Homo* and *Pongo*, the platyrrhines *Ateles* and *Alouatta*, and the cercopithecoids *Theropithecus* and *Piliocolobus*).

409 The slightly dissimilar bgPC3 scores for the two *Epipliopithecus* individuals result from
410 differences in orientation between the posterior and anterior canals (obtuse angle in
411 NHMW 1970/1397/0003 vs. right angle in NMB OE 303; SOM Fig. S2), causing a wider
412 separation between the lateral and posterior canals (Fig. 4a–c).

413 When the three bgPCs are considered together, the two *Epipliopithecus* individuals
414 show the greatest morphological similarities with platyrrhines (less so in NHMW
415 1970/1397/0003), as demonstrated by Mahalanobis distances from group centroids and by
416 their posterior probabilities of group membership (Table 3), leading us to reject close
417 similarities to the remaining groups for NMB OE 303, and to all anthropoid groups for
418 NHMW 1970/1397/0003 ($p < 0.05$). *Aegyptopithecus*, *Parapithecus*, *Oreopithecus*, and
419 stem platyrrhines also closely resemble extant New World monkeys, with *Oreopithecus*
420 also showing marginal affinities with cercopithecoids (Table 3). We obtain very similar
421 results when considering all catarrhines as a single group, with all fossils being classified
422 as platyrrhines (Table 4). For *Oreopithecus* and NHMW 1970/1397/0003, group
423 membership for catarrhines cannot be rejected. However, both specimens show much
424 lower Mahalanobis distances to the platyrrhine centroid (almost three times) than to that of
425 catarrhines. The two *Epipliopithecus* individuals are closer to one another than they are to
426 other fossil taxa (except for one individual of *Homunculus*, MPM-PV 3501), in turn showing
427 similarities with stem platyrrhines, *Aegyptopithecus* and *Oreopithecus* (Table 5). A cluster
428 analysis based on the momenta of the deformation fields confirms these results (Fig. 7).
429 *Epipliopithecus* clusters with *Alouatta* and *Ateles* (large and rounded vertical canals and a
430 large gap between the lateral and posterior canals), as well as *Pithecia* (obtuse angle
431 formed by the anterior and posterior canals), within a larger cluster that includes the
432 remaining extant platyrrhines and the other fossil taxa included in the analysis. In
433 particular, *Aegyptopithecus* and *Homunculus* cluster with *Saimiri* and *Cebus* (flat lateral
434 canal and similarities in the anterior canal morphology), while *Oreopithecus* clusters with

435 *Callicebus* (orientation of the anterior and posterior canals). Hylobatids cluster within a
436 larger group that also includes most cercopithecoids, and extant great apes cluster
437 together due to their distinctive stout volumetric proportions (Urciuoli et al., 2020).
438
439 *3.3. Phylogenetic signal and phylomorphospace*
440 Like previous analyses (Urciuoli et al., 2020; del Rio et al., 2020; Morimoto, et al.,
441 2020, our results indicate that the vestibule and SCs embed significant phylogenetic signal
442 (K_{mult} = 1.134, $p < 0.001$), suggesting these traits conform to a Brownian motion model of
443 evolution, with closely related taxa resembling one another slightly more than expected
444 ($K_{mult} > 1$). The phylogenetic signal computed for each bgPC separately is significant in all
445 instances (Table 6), with bgPC1 and bgPC2 suggesting the same evolutionary mode as
446 K_{mult} ($K > 1$). Conversely, we observe that the variance accumulates within clades for
447 bgPC3 ($K < 1$), thus suggesting that changes along this axis might be more strongly
448 affected by homoplasy.
449 The phylogenetic signal detected justifies the application of the phylomorphospace
450 approach (Fig. 8). The results indicate that the reconstructed LCAs of crown anthropoids
451 (Fig. 9a) and crown catarrhines (Fig. 9c) fall within the variability of extant New World
452 monkeys, being very close to the platyrrhine LCA (Fig. 9b)—irrespective of the
453 phylogenetic hypothesis used in the analysis for *Epipliopithecus* (i.e., stem catarrhine vs.
454 stem hominoid, Figs. 3 and 8; SOM Fig. S3). Cercopithecoids and hominoids appear much
455 more derived in SC morphology than platyrrhines, but in different directions. The crown
456 anthropoid, crown platyrrhine and crown catarrhine LCAs are reconstructed as possessing
457 large and slightly vertically-elongated canals (more so in the crown anthropoid and crown
458 platyrrhine LCAs; Fig. 9a, b) coupled with a long CC (shorter in the crown catarrhine LCA;
459 Fig. 9c), intermediate volumetric proportions (similar to those found in New World monkeys
460 and cercopithecins; Fig. 10), and a coplanar lateral canal that does not intersect the plane

461 of the posterior one (Fig. 9a–c). The LCA of crown catarrhines also shows a slightly more
462 superiorly bent ampullary portion, more so than in *Epipliopithecus* (Fig. 9c). In contrast, the
463 reconstructed crown hominoid LCA (Fig. 9d) is found in an area of the morphospace
464 devoid of extant taxa and, according to our estimation, it already displayed some derived
465 characters that are not found in *Epipliopithecus* (i.e., moderately vertically-compressed
466 anterior canal, stouter canal proportions, lateral ampulla connecting more superiorly with
467 the vestibule).

468 From a phenetic viewpoint, based on weighted Euclidean distances between
469 *Epipliopithecus* and the bgPC scores for the reconstructed LCAs (Table 7), the former
470 taxon is most similar to the crown catarrhine ancestral condition, and also closer to the
471 crown anthropoid and platyrrhine LCAs, than to the ancestral conditions reconstructed for
472 either hominoids or cercopithecoids.

473 We further synthesized the information provided by the phylomorphospace
474 approach by defining seven discrete characters coded in a cladistic fashion (Table 8; Fig.
475 11). Their coding for the reconstructed LCAs as well as both extant and extinct
476 anthropoids included in the analyses is reported in Table 9 and SOM Table S4. When the
477 character states for extinct and extant taxa are analyzed against the two phylogenetic
478 hypotheses by considering parsimony as a criterion (Table 10), *Epipliopithecus* is more
479 parsimoniously interpreted as a stem catarrhine (Fig. 3a) than as a stem hominoid (Fig.
480 3b). The phylogenetic implications of the seven coded characters (Fig. 11; Tables 8 and 9;
481 SOM Table S4) are discussed below and illustrated in Figure 12.

482 <u>Size of the vestibule relative to the semicircular canals</u> Extant hominids differ from all the
483 remaining extant taxa in possessing a relatively larger vestibule, which may be thus
484 interpreted as a synapomorphy of at least crown hominids. Among the extinct taxa, only
485 the purported stem hominoid *Oreopithecus* displays the derived hominid condition,
486 indicating either an independent acquisition of this feature in this taxon (as supported by

our LCA reconstructions) or a secondary reversal in hylobatids. *Epipliopithecus*, in any case, retains the plesiomorphic condition of nonhominoid anthropoids.

Robusticity of the semicircular canals This character has the same distribution as the size of the vestibule relative to the SCs. Extant hominids and *Oreopithecus* differ from the remaining taxa by displaying stouter proportions. Accordingly, such proportions might be interpreted either as convergent between *Oreopithecus* and hominids, or as a hominoid synapomorphy with subsequent reversal in hylobatids. Our LCA reconstructions do not provide clear support for either possibility, as they suggest an intermediate ancestral condition in the overlap zone between hominoids and nonhominoid catarrhines. In either case, for this character *Epipliopithecus* displays the more plesiomorphic condition of nonhominoid anthropoids.

Shape of the anterior semicircular canal This character is more variable than the preceding ones, both within anthropoid subclades, and sometimes even within the same species. However, extant catarrhines generally differ from platyrrhines by possessing an anterior canal that is not superiorly elongated, being instead either rounded (as in humans and most cercopithecoids) or vertically compressed (as in great apes and generally hylobatids, although in the latter it varies intraspecifically between rounded and vertically compressed). Our LCA reconstructions suggest that the ancestral anthropoid condition—a superiorly elongated anterior canal—is symplesiomorphic not only for platyrrhines but also for the stem catarrhine *Aegyptopithecus*. They further support the view that a rounded anterior SC is synapomorphic of crown catarrhines, while a vertically compressed anterior SC would be synapomorphic for crown hominoids + *Oreopithecus*. In this regard, *Epipliopithecus* is more derived than *Aegyptopithecus* but less so than *Oreopithecus*. This character, therefore, unambiguously supports for *Epipliopithecus* a catarrhine status more derived than in *Aegyptopithecus*, although it would be consistent with either a stem catarrhine or a stem hominoid status.

513 Shape of the anterior portion of the semicircular canal Hylobatids and orangutans differ
514 from the rest of the sample by displaying an anterosuperiorly-projecting anterior portion of
515 the anterior canal. This condition may be interpreted as a crown hominoid synapomorphy
516 subsequently reversed in hominines, as further supported by the fact that *Oreopithecus*
517 displays the derived condition for hominoids. Alternatively, this feature might have been
518 independently acquired in *Oreopithecus*, as suggested by our LCA reconstructions, which
519 only recover it as a hylobatid synapomorphy. Given the possession of other SC hominoid
520 synapomorphies in *Oreopithecus*, we tend to favor the former interpretation, even if both
521 are equally parsimonious. In any case, *Epipliopithecus* retains the more plesiomorphic
522 condition of non-hominoid anthropoids.
523 Shape of the posterior semicircular canal Although this character is somewhat variable
524 within anthropoid subclades and sometimes even within species, some generalities can be
525 drawn. In platyrrhines, the posterior canal is generally elongated superiorly to some extent,
526 whereas most cercopithecoids have a rounded posterior canal, and hominoids generally
527 vary between a rounded and a vertically compressed morphology (only sometimes
528 superiorly elongated in *Pan*). Our LCA reconstructions indicate that platyrrhines and
529 *Aegyptopithecus* retain the ancestral anthropoid condition (superiorly elongated posterior
530 canal), whereas the rounded morphology would be synapomorphic for crown hominoids.
531 *Epipliopithecus* displays the plesiomorphic anthropoid condition and thus differs from
532 *Oreopithecus*, which displays the derived catarrhine morphology.
533 Shape of the lateral semicircular canal ampullary portion Extant hominoids differ from the
534 remaining extant taxa and all the analyzed extinct genera by displaying a markedly
535 superiorly-bent ampullary portion of the lateral canal. Both *Epipliopithecus* and
536 *Oreopithecus* thus display a more plesiomorphic condition than crown hominoids, as
537 further confirmed by our LCA reconstructions.

538 Length of the common crus This character is also variable to some extent, but platyrrhines
539 generally display a longer CC than extant catarrhines, with hominoids having an even
540 shorter CC than most cercopithecoids. Our LCA reconstructions support an intermediate
541 length of the CC as synapomorphic of crown catarrhines, with a short CC being
542 synapomorphic for hominoids. *Epipliopithecus* resembles *Aegyptopithecus* and
543 platyrrhines by retaining the ancestral anthropoid condition, whereas *Oreopithecus*
544 displays the derived hominoid morphology.
545
546 **4. Discussion**
547 Our analysis of the SC and vestibule morphology of *Epipliopithecus* allows us to
548 refine our understanding of the evolution of this anatomical region in anthropoid primates
549 and to refine previous hypotheses proposed by Urciuoli et al. (2020). The results of our
550 deformation-based 3DGM analysis and the reconstruction of ancestral morphotypes for
551 main anthropoid clades indicate that, like the stem catarrhine *Aegyptopithecus*,
552 *Epipliopithecus* displays a platyrrhine-like morphology most similar to that reconstructed
553 for the crown catarrhine LCA. This might be compatible with *Epipliopithecus* being either a
554 stem catarrhine, or a crown catarrhine only slightly postdating the cercopithecoid-hominoid
555 split. However, the fact that *Epipliopithecus* most closely resembles the crown anthropoid
556 (and platyrrhine) LCAs (Table 7) suggests that the semicircular morphology of this taxon is
557 most consistent with its status as a stem catarrhine. This conclusion is further supported
558 by the analysis of seven discrete characters coded for this anatomical area—which
559 indicate that this is the most parsimonious hypothesis, for reasons discussed in greater
560 detail below.
561
562 *4.1.* Epipliopithecus *as a hominoid*

Based on the morphology of the SCs and vestibule, *Epipliopithecus* lacks multiple hominoid synapomorphies, including a large vestibule relative to the canals, stout SCs, vertically-compressed anterior canal, anterosuperiorly- projecting anterior portion of the anterior canal, markedly superiorly-bent ampullary portion of the lateral canal, and short CC. Urciuoli et al.(2020) already interpreted some of these features (vertically-compressed anterior canal and markedly superiorly-bent ampullary portion of the lateral canal) as potential crown hominoid synapomorphies, whereas they interpreted others (large vestibule and stout canals) as hominid synapomorphies. Urciuoli et al. (2020) interpreted a superiorly-bent ampullary portion of the lateral canal as a hominoid synapomorphy. However, hominoids are, in fact, characterized by the possession of a markedly bent trajectory, whereas other catarrhines display a flat to slightly superiorly-bent ampullary portion of the lateral canal. This is the case for *Epipliopithecus*, which displays much less bending of the lateral canal than in *Oreopithecus* or any extant hominoid.

The possession of a large vestibule and stout canals was previously interpreted as being synapomorphic for hominids (Urciuoli et al., 2020) because hylobatids display a different (‘monkey-like’) condition. The differences in volumetric proportions between *Epipliopithecus* and hominids are particularly clear (Fig. 10), with the former closely resembling platyrrhines, *Aegyptopithecus*, and the inferred ancestral catarrhine condition. Given that both features are present in *Oreopithecus*, they may be interpreted as hominoid synapomorphies subsequently reversed in hylobatids—thereby supporting a more basal branching for *Epipliopithecus*. However, their interpretation as hominid synapomorphies is equally parsimonious, as it would only imply their independent acquisition in *Oreopithecus*. Therefore, neither a large vestibule nor stout canals can be used to unambiguously discount a hominoid status for *Epipliopithecus*. A similar caveat applies to the lack of an anterosuperiorly-projecting anterior canal in *Epipliopithecus*. This condition was previously interpreted as an autapomorphy of *Hylobates* (Le Maître, et al., 2017) or as a hylobatid

589 synapomorphy (Spoor and Zonneveld, 1998; Urciuoli, et al. 2020). However, given its
590 presence in orangutans and *Oreopithecus*, it is more readily interpreted as a hominoid
591 synapomorphy subsequently reversed in hominines. The interpretation of some of the
592 potential hominoid synapomorphies lacking in *Epipliopithecus* is ambiguous due to
593 homoplasy (convergence and/or reversal). However, it is worth noting that, except for the
594 markedly superiorly bent ampullary portion of the lateral canal, *Oreopithecus* further
595 displays two more unambiguous hominoid synapomorphies (vertically compressed anterior
596 canal and short CC). The absence of these features in *Epipliopithecus* thus conclusively
597 excludes a more derived hominoid status for the latter as compared with *Oreopithecus*.
598 *Epipliopithecus* also displays some hylobatid-like features in the spatial
599 configuration between the lateral and posterior canals, as well as in the orientation
600 between the anterior and posterior canals. According to Urciuoli et al. (2020), the lack of
601 intersection between the lateral and posterior canals and the presence of an obtuse angle
602 between the anterior and posterior canals would be synapomorphic for hominoids and
603 hylobatids, respectively. However, only *Hylobates* consistently displays both features,
604 while most anthropoid taxa, as well as the two *Epipliopithecus* individuals, show a
605 considerable amount of intraspecific variation. Hence, we refrained from coding these
606 features in a cladistic manner, especially in view of the low phylogenetic signal ($K < 1$)
607 recovered for bgPC3 (accounting for the variation in the configuration of these features),
608 which suggests a substantial degree of homoplasy. Indeed, previous analyses
609 hypothesized that suspensory species possess more obtuse angles between the vertical
610 canals (Gonzales et al., 2019), as this configuration provides an increased sensitivity for
611 pitch (at the expense of roll) head movements (Muller and Verhagen, 2002a,b,c). The
612 similarities between NHMW 1970/1397/0003, hylobatids, and some atelids (Spoor and
613 Zonneveld, 1998; Gonzales et al., 2019) would thus agree with previous inferences about
614 the locomotor repertoire of this taxon including some degree of suspensory behaviors

615 (Zapfe, 1958; Fleagle, 1983; Langdon, 1986; Rose, 1994; Arias Martorell et al., 2015). In
616 contrast, the more plesiomorphic condition of NBM OE 303III (characterized by tangent
617 lateral and posterior canals, and vertical canals approximating a right angle), also found in
618 *Aegyptopithecus* and some nonsuspensory platyrrhine species, suggests caution when
619 using SC orientation alone for inferring positional behaviors (Perier et al., 2016; contra
620 Malinzak et al., 2012; Berlin et al., 2013).
621
622 *4.2.* Epipliopithecus *as a stem catarrhine*
623 *Epipliopithecus* resembles both stem platyrrhines and the stem catarrhine
624 *Aegyptopithecus* in lacking all of the aforementioned hominoid synapomorphies, thereby
625 retaining the plesiomorphic anthropoid condition—a relatively small vestibule, slender SCs,
626 anterosuperiorly nonprojecting anterior portion of the anterior canal, superiorly elongated
627 posterior canal, ampullary portion of the lateral canal not markedly bent superiorly, and
628 long CC. The fact that *Epipliopithecus* lacks hominoid synapomorphies displayed by
629 *Oreopithecus* could still be consistent with a more basal stem hominoid status. However,
630 such an interpretation is contradicted by the retention in *Epipliopithecus* of a superiorly
631 elongated posterior canal and a long CC—contrasting with the rounded posterior canal
632 and moderately short CC that are synapomorphic of crown catarrhines. The catarrhine
633 status of *Epipliopithecus* and other pliopithecoids is well established based on multiple
634 features, such as the loss of the second premolars and the presence of a C^1/P_3 honing
635 complex (e.g., Harrison, 2013). The catarrhine status of *Epipliopithecus* is further
636 supported by the possession of a rounded anterior canal, which is intermediate between
637 the primitive morphology (superiorly elongated anterior canal) retained by platyrrhines and
638 *Aegyptopithecus*, and the more derived (vertically compressed) morphology
639 synapomorphic of hominoids. In this regard, *Epipliopithecus* is more derived toward crown
640 catarrhines than the propliopipithecoid *Aegyptopithecus*, in agreement with other cranial

features such as the possession of a partially enclosed tubular ectotympanic in *Epipliopithecus* (e.g., Harrison, 2013).

In summary, based on the morphology of the SCs and vestibule, *Epipliopithecus* is most parsimoniously interpreted as a stem catarrhine more derived than *Aegyptopithecus*, due to its possession of a crown catarrhine synapomorphy—rounded anterior canal—coupled with the lack of two additional crown catarrhine synapomorphies (superiorly elongated posterior canal and long CC) and multiple hominoid and/or hominid synapomorphies as described above. The shapes of the anterior and posterior canals and CC should be considered with caution in light of the intraspecific variability displayed by these characters in some taxa (SOM Table S4). Previous analyses noted a structural relationship between the morphology of these canals and the extension of the subarcuate fossa (Jeffery and Spoor, 2006; Jeffery et al., 2008), and this relationship has been uncritically assumed in some studies (Spoor et al., 2007; Silcox et al., 2009; Gonzales et al., 2019). However, in most cases the fossa simply expands within the space left available from the ossification of the canals, with little or no influence on their shape (Jeffery et al., 2008; see also Urciuoli et al., 2020). In support of the latter hypothesis, we observe meager dissimilarities in the anterior canal morphology of NHMW 1970/1397/0003 and NBM OE 303III—except for the angle, as discussed above—irrespective of the marked differences in the morphology of the fossa between the two individuals (Zapfe, 1960). While a large amount of morphological variation has been documented within ruminant genera (Mennecart and Costeur, 2016), variation in CC length and shape has not been exhaustively analyzed in primates (Spoor and Zonneveld, 1998; Ekdale 2013; Lee et al., 2013). In the present study, we found considerable intraspecific variation in CC length for some species of monkeys and apes. Nevertheless, our results support a clear morphocline from the ancestral condition (long CC) retained by platyrrhines, *Aegyptopithecus*, and *Epipliopithecus*, to the most derived condition (short CC) characteristic of hominoids, with

667 cercopithecoids displaying an intermediate condition that is likely synapomorphic for crown
668 catarrhines as a whole. Therefore, *Epipliopithecus* SC morphology supports its
669 interpretation as more derived than *Aegyptopithecus* toward crown catarrhines, but
670 excludes a crown catarrhine status and, in particular, a closer relationship with hominoids
671 (unlike in the case of *Oreopithecus*).
672
673 **5. Conclusions**
674 Our results are in broad agreement with previous analyses suggesting that
675 *Epipliopithecus* displays a 'typical monkey' inner ear morphology (Morimoto et al., 2020),
676 while *Oreopithecus* possesses SC and vestibule features derived toward the crown
677 hominoid condition (Urciuoli et al., 2020). At the same time, our study further refines
678 previous comparisons of SC and vestibule morphology between *Epipliopithecus* and other
679 anthropoids, enabling us to test competing hypotheses about the phylogenetic position of
680 this taxon (i.e., stem catarrhine vs. stem hominoid).
681 From a phenetic viewpoint, for this anatomical area *Epipliopithecus* more closely
682 resembles platyrrhines and the stem catarrhine *Aegyptopithecus*, as well as the
683 reconstructed ancestral catarrhine morphotype. The fact that *Epipliopithecus* shows
684 greater similarities with the platyrrhine and anthropoid ancestral morphotypes, rather than
685 with those of cercopithecoids or hominoids, supports the view that *Epipliopithecus* is a
686 stem catarrhine instead of a stem hominoid. From a cladistic perspective, this
687 interpretation is confirmed based on a series of crown catarrhine and crown hominoid
688 synapomorphies. *Epipliopithecus* is more parsimoniously interpreted as a stem catarrhine
689 than as a stem hominoid based on the vestibular morphology analyzed here because it
690 lacks several catarrhine and all hominoid synapomorphies. Specifically, the possession of
691 a rounded posterior canal reinforces the view that *Epipliopithecus* is more derived than
692 *Aegyptopithecus* among stem catarrhines.

693 The information provided by the SCs and vestibule is thus congruent with the
694 ectotympanic morphology of *Epipliopithecus* (see review in Fricano, 2018), which is more
695 plesiomorphic than in crown catarrhines but more derived than in propliopithecoids. Some
696 similarities between *Epipliopithecus* and hylobatids are based on characters that are too
697 variable within species to be of use for phylogenetic assessment. Such features might
698 have evolved independently between some atelids and hylobatids, due to similar
699 locomotor-related selection pressures, and do not support the close phylogenetic link
700 classically hypothesized between pliopithecoids and hylobatids (Hürzeler, 1954; Zapfe,
701 1960, 1961; Simons and Fleagle, 1973), particularly given that *Epipliopithecus* displays no
702 crown hominoid synapomorphies. We therefore conclude that the SC and vestibular
703 morphology reinforces the most commonly held view that, in accordance with most
704 (Zalmout et al., 2010; Stevens et al., 2013; Nengo et al., 2017) but not all (Alba et al.,
705 2015) recent cladistic analyses, *Epipliopithecus* is best interpreted as a stem catarrhine
706 rather than a stem hominoid.
707
708 **References**
709 Adams, D.C., 2014. A generalized K statistic for estimating phylogenetic signal from shape
710 and other high-dimensional multivariate data. Syst. Biol. 63, 685–697.
711 Adams D.C, Collyer, M.L., Kaliontzopoulou, A., 2019. Geomorph: Software for geometric
712 morphometric analyses. R Package Version.
713 https://cran.rproject.org/package=geomorph.
714 Alba, D.M., Berning, B., 2013. On the holotype and original description of the pliopithecid
715 *Plesiopliopithecus lockeri* (Zapfe, 1960). J. Hum. Evol. 65, 338–340.
716 Alba, D.M., Moyà-Solà, S., 2012. A new pliopithecid genus (Primates: Pliopithecoidea)
717 from Castell de Barberà (Vallès-Penedès Basin, Catalonia, Spain). Am. J. Phys.
718 Anthropol. 147, 88–112.

719 Alba, D.M., Moyà-Solà, S., Malgosa, A., Casanovas-Vilar, I., Robles, J.M., Almécija, S.,
720 Galindo, J., Rotgers, C., Bertó Mengual, J.V., 2010. A new species of *Pliopithecus*
721 Gervais, 1849 (Primates: Pliopithecidae) from the Middle Miocene (MN8) of Abocador
722 de Can Mata (els Hostalets de Pierola, Catalonia, Spain). Am. J. Phys. Anthropol. 141,
723 52–75.
724 Alba, D.M., Almécija, S., DeMiguel, D., Fortuny, J., Pérez de los Ríos, M., Pina, M.,
725 Robles, J. M., Moyà-Solà, S., 2015. Miocene small-bodied ape from Eurasia sheds
726 light on hominoid evolution. Science 350, aab2625.
727 Almécija, S., Tallman, L., Sallam, H.M., Fleagle, J.G., Hammond, A.S., Seiffert, E.R.,
728 2019. Early anthropoid femora reveal divergent adaptive trajectories in catarrhine hind-
729 limb evolution. Nat. Commun. 10, 4778.
730 Andrews, P.J., Harrison, T., Delson, E., Bernor, R.L., Martin, L., 1996. Distribution and
731 biochronology of European and Southwest Asian Miocene catarrhines. In: Bernor,
732 R.L., Fahlbusch, V., Mittmann, H. (Eds.), The Evolution of Western Eurasian Neogene
733 Mammalian Faunas. Columbia University Press, New York, pp. 168–207.
734 Ankel, F., 1965. Der Canalis Sacralis als Indikator für die Länge der Caudalregion der
735 Primaten. Folia Primatol. 3, 263–276.
736 Arias-Martorell, J., Alba, D.M., Potau, J. M., Bello-Hellegouarch, G., Pérez-Pérez, A.,
737 2015. Morphological affinities of the proximal humerus of *Epipliopithecus*
738 *vindobonensis* and *Pliopithecus antiquus*: Suspensory inferences based on a 3D
739 geometric morphometrics approach. J. Hum. Evol. 80, 83–95.
740 Arnold, C., Matthews, L.J., Nunn, C.L., 2010. The 10kTrees website: A new online
741 resource for primate phylogeny. Evol. Anthropol. 19, 114–118.
742 Beaudet, A., Dumoncel, J., Thackeray, J.F., Bruxelles, L., Duployer, B., Tenailleau, C.,
743 Bam, L., Hoffman, J., de Beer, F., Braga, J., 2016. Upper third molar internal structural

744 organization and semicircular canal morphology in Plio-Pleistocene South African
745 cercopithecoids. J. Hum. Evol. 95, 104–120.
746 Begun, D.R., 2002 The Pliopithecoidea. In: Hartwig, W.C. (Ed.), 2002. The Primate Fossil
747 Record. Cambridge University Press, Cambridge, pp. 221–240.
748 Begun, D.R., 2017. Evolution of the Pliopithecoidea. In A. Fuentes (Ed.), *The International*
749 *Encyclopedia of Primatology* (pp. [1-4]): John Wiley & Sons.
750 Berlin, J.C., Kirk, E.C., Rowe, T.B., 2013. Functional implications of ubiquitous
751 semicircular canal non-orthogonality in mammals. PLoS One 8, e79585.
752 Billet, G., Hautier, L., Lebrun, R., 2015. Morphological diversity of the bony labyrinth (inner
753 ear) in extant xenarthrans and its relation to phylogeny. J. Mammal. 96, 658–672.
754 Blomberg, S.P., Garland, T., Ives, A.R., 2003. Testing for phylogenetic signal in
755 comparative data: behavioral traits are more labile. Evolution 57, 717–745.
756 Bône, A., Louis, M., Martin, B., Durrleman, S., 2018. Deformetrica 4: an open-source
757 software for statistical shape analysis. In: Reuter, M., Wachinger, C., Lombaert, H.,
758 Paniagua, B., Lüthi, M., Egger, B. (Eds.), Shape in Medical Imaging. Shape MI 2018.
759 Springer, Cham, pp. 3–13.
760 Bookstein, F.L., 2019. Pathologies of between-groups principal components analysis in
761 geometric morphometrics. Evol. Biol. 46, 271–302.
762 Braga, J., Samir, C., Risser, L., Dumoncel, J., Descouens, D., Thackeray, J.F., Barlesque,
763 P., Oettlé, A., Loubes, J.-M., Fradi, A., 2019a. Cochlear shape reveals that the human
764 organ of hearing is sex-typed from birth. Sci. Rep. 9, 10889.
765 Bush, E.C., Simons, E.L., Dubowitz, D.J., Allman, J.M., 2004. Endocranial volume and
766 optic foramen size in *Parapithecus grangeri*. In: Ross, C.F., Kay, R.F. (Eds),
767 Anthropoid Origins: New Visions. Kluwer/Plenum, New York, pp. 603–614.
768 Cardini, A., O'Higgins, P., Rohlf, F.J., 2019. Seeing distinct groups where there are none:
769 Spurious patterns from between-group PCA. Evol. Biol. 46, 303–316.

770 Cardini, A., Polly, P.D., 2020. Cross-validated between-group PCA scatterplots: A solution
771 to spurious group separation? Evol. Biol. 47, 85–95.
772 Casanovas-Vilar, I., Alba, D.M., Garcés, M., Robles, J.M., Moyà-Solà, S., 2011. Updated
773 chronology for the Miocene hominoid radiation in Western Eurasia. Proc. Natl. Acad.
774 Sci. USA 108, 5554–5559.
775 Ciochon, R.L., Corruccini, R.S., 1977. The phenetic position of *Pliopithecus* and its
776 phylogenetic relationship to the Hominoidea. Syst. Zool. 26, 290–299.
777 Coleman, M.N., Colbert, M.W. 2010. Correlations between auditory structures and hearing
778 sensitivity in non-human primates. J. Morphol. 271, 511–532.
779 Costeur, L., Grohé, C., Aguirre-Fernández, G., Ekdale, E., Schulz, G., Müller, B.,
780 Mennecart, B., 2018. The bony labyrinth of toothed whales reflects both phylogeny
781 and habitat preferences. Sci. Rep. 8, 7841.
782 David, R., Droulez, J., Allain, R., Berthoz, A., Janvier, P., Bennequin, D., 2010. Motion
783 from the past. A new method to infer vestibular capacities of extinct species. C.R.
784 Palevol 9, 397–410.
785 David, R., Stoessel, A., Berthoz, A., Spoor, F., Bennequin, D., 2016. Assessing
786 morphology and function of the semicircular duct system: introducing new in-situ
787 visualization and software toolbox. Sci. Rep. 6, 32772.
788 del Rio, J., Aristide, L., dos Reis, S.F., dos Santos, T.M.P., Lopes, R.T., Perez, S.I., 2020.
789 Allometry, function and shape diversification in the inner ear of platyrrhine primates. J.
790 Mammal. Evol. https://doi.org/10.1007/s10914-019-09490-9.
791 Delson, E., Andrews, P.J., 1975. Evolution and interrelationships of the catarrhine
792 primates. In: Luckett, W.P., Szalay, F.S. (Eds.), Phylogeny of the Primates: A
793 Multidisciplinary Approach. Plenum Press, New York, pp. 405–446.

794 Dumoncel, J., Durrleman, S., Braga, J., Jessel, J.P., Subsol, G., 2014. Landmark-free 3D
795 method for comparison of fossil hominins and hominids based on endocranium and
796 EDJ shapes. Am. J. Phys. Anthropol. 153 (S58), 110.
797 Durrleman, S., Pennec, X., Trouvé, A., Ayache, N., Braga, J., 2012. Comparison of the
798 endocranial ontogenies between chimpanzees and bonobos via temporal regression
799 and spatiotemporal registration. J. Hum. Evol. 62, 74–88.
800 Durrleman, S., Prastawa, M., Korenberg, J.R., Joshi, S., Trouvé, A., Gerig, G., 2012.
801 Topology preserving atlas construction from shape data without correspondence using
802 sparse parameters. In: Ayache, N., Delingette, H., Golland, P., Mori, K. (Eds.), Medical
803 Image Computing and Computer-Assisted Intervention – MICCAI 2012. Springer,
804 Berlin, pp. 223–230.
805 Ekdale, E.G., 2013. Comparative anatomy of the bony labyrinth (inner ear) of placental
806 mammals. PLoS One 8, e66624.
807 Farris, J.S., 1989. The retention index and the rescaled consistency index. Cladistics 5,
808 417–419.
809 Fleagle, J.G., 1983. Locomotor adaptations of Oligocene and Miocene hominoids and their
810 phyletic implications. In: Ciochon, R.L., Corruccini, R.S. (Eds.), New Interpretations of
811 Ape and Human Ancestry. Plenum Press, New York, pp. 301–324.
812 Fleagle, J.G., 1984. Are there any fossil gibbons? In: Preuschoft, H., Chivers, D.J.,
813 Brockelman, W.Y., Creel, N. (Eds.), The Lesser Apes: Evolutionary and Behavioral
814 Biology. Edinburgh University Press, Edinburgh, pp. 431–447.
815 Fricano, E.E.I., 2018. The primate ectotympanic tube: correlates of structure, function, and
816 development. Ph.D. Dissertation, Johns Hopkins University.
817 Fulwood, E.L., Boyer, D.M., Kay, R.F., 2016. Stem members of Platyrrhini are distinct from
818 catarrhines in at least one derived cranial feature. J. Hum. Evol. 100, 16–24.

Gilbert, C.C., Ortiz, A., Pugh, K.D., Campisano, C.J., Patel, B.A., Singh, N.P., Fleage, J.G., Patnaik, R., 2020. New middle Miocene ape (Primates: Hylobatidae) from Ramnagar, India fills major gaps in the hominoid fossil record. Proc. R. Soc. B 287, 20201655.

Glaunès, J.A., Joshi, S., 2006. Template estimation form unlabeled point set data and surfaces for Computational Anatomy. in: Pennec, X., Joshi, S. (Eds.), MICCAI 2006 Workshop Proceedings. MFCA'06 Workshop. Mathematical Foundations of Computational Anatomy: Geometrical and Statistical Methods for Modelling Biological Shape Variability. INRIA/MICCAI, Conpenhagen, pp. 29–39.

Gonzales, L.A., Malinzak, M.D., Kay, R.F., 2019. Intraspecific variation in semicircular canal morphology—A missing element in adaptive scenarios? Am. J. Phys. Anthropol. 168, 10–24.

Grohé, C., Tseng, Z. J., Lebrun, R., Boistel, R., Flynn, J.J., 2015. Bony labyrinth shape variation in extant Carnivora: a case study of Musteloidea. J. Anat. 228, 366–383.

Grohé, C., Lee, B., Flynn, J.J., 2018. Recent inner ear specialization for high-speed hunting in cheetahs. Sci. Rep. 8, 1–8.

Harrison, T., 1982. Small-bodied apes from the Miocene of East Africa. Ph.D. Dissertation, University College London.

Harrison, T., 1987. The phylogenetic relationships of the early catarrhine primates: a review of the current evidence. J. Hum. Evol. 16, 41–80.

Harrison, T., 2005. The zoogeographic and phylogenetic relationships of early catarrhine primates in Asia. Anthropol. Sci. 113, 43–51.

Harrison, T., 2010. Dendropithecoidea, Proconsuloidea, and Hominoidea (Catarrhini, Primates). In: Werdelin, L. (Ed.), Cenozoic Mammals of Africa. University of California Press, Berkeley, pp. 429–469.

Harrison, T., 2013. Catarrhine origins. In: Begun, D.R. (Ed.), A Companion to Paleoanthropology. Blackwell Publishing, Oxford, pp. 376–396.

Harrison, T., Gu, Y., 1999. Taxonomy and phylogenetic relationships of early Miocene catarrhines from Sihong, China. J. Hum. Evol. 37, 225–277.

Harrison, T., Zhang, Y., Wei, G., Sun, C., Wang, Y., Liu, J., Tong, H., Huang, B., Xu, F., 2020. A new genus of pliopithecoid from the late Early Miocene of China and its implications for understanding the paleozoogeography of the Pliopithecoidea. J. Hum. Evol. 145, 102838.

Harzhauser, M., Kroh, A., Mandic, O., Piller, W. E., Göhlich, U., Reuter, M., Berning, B., 2007. Biogeographic responses to geodynamics: A key study all around the Oligo–Miocene Tethyan Seaway. Zool. Anz. 246, 241–256.

Hürzeler, J., 1954. Contribution a l'odontologie et a la phylogénèse du genre *Pliopithecus* Gervais. Ann. Paleontol. 40, 5–63.

Jeffery, N., Spoor, F., 2006. The primate subarcuate fossa and its relationship to the semicircular canals part I: prenatal growth. J. Hum. Evol. 51, 537–549.

Jeffery, N., Ryan, T.M., Spoor, F., 2008. The primate subarcuate fossa and its relationship to the semicircular canals part II: Adult interspecific variation. J. Hum. Evol. 55, 326–339.

Kay, R.F., Simons, E., Ross, J.L., 2009a. The basicranial anatomy of African Eocene/Oligocene anthropoids. Are there any clues for platyrrhine origins? In: Fleagle, J.G., Gilbert, C.C. (Eds.), Elwyin Simons: A Search for Origins. Springer, New York, pp. 125–158.

Kay, R.F., Fleagle, J.G., Mitchell, T.R.T., Colbert, M., Bown, T., Powers, D.W., 2009b. The anatomy of *Dolichocebus gaimanensis*, a stem platyrrhine monkey from Argentina. J. Hum. Evol. 54, 323–382.

869 Kay, R.F., 2015. Biogeography in deep time – What do phylogenetics, geology, and
870 paleoclimate tell us about early platyrrhine evolution? Mol. Phylogenet. Evol. 82, 358–
871 374.
872 Kirk, E.C., Gosselin-Ildari, A.D., 2009. Cochlear labyrinth volume and hearing abilities in
873 primates. Anat. Rec. 292, 765–776.
874 Kunimatsu, Y., Nakatsukasa, M., Shimizu, D., Nakano, Y., Ishida, H., 2019. Loss of the
875 subarcuate fossa and the phylogeny of *Nacholapithecus*. J. Hum. Evol. 131, 22–27.
876 Langdon, J.H., 1986. Functional morphology of the Miocene hominoid foot. Contrib.
877 Primatol. 22, 239e257.
878 Lebrun, R., P. de León, M., Tafforeau, P., Zollikofer, C., 2010. Deep evolutionary roots of
879 strepsirrhine primate labyrinthine morphology. J. Anat 216, 368–380.
880 Lebrun, R., Godinot, M., Couette, S., Tafforeau, P., Zollikofer, C., 2012. The labyrinthine
881 morphology of *Pronycticebus gaudryi* (Primates, Adapiformes). Palaeobiodiv.
882 Palaeoenvir. 92, 527–537.
883 Lee, J.Y., Shin, K.J., Kim, J.N., Yoo, J.Y., Song, W.C., Koh, K.S., 2013. A morphometric
884 study of the semicircular canals using micro-CT images in three-dimensional
885 reconstruction. Anat. Rec. 269, 834–839.
886 Le Maître A., Schuetz, P., Vignaud, P., Brunet, M.., 2017. New data about semicircular
887 canal morphology and locomotion in modern hominoids. J. Anat. 231, 95–109.
888 Macrini, T.E., Flynn, J.J., Ni, X., Croft, D.A., Wyss, A. R., 2013. Comparative study of
889 notoungulate (Placentalia, Mammalia) bony labyrinths and new phylogenetically
890 informative inner ear characters. J. Anat. 223, 442–461.
891 Malinzak, M.D., Kay, R.F., Hullar, T.E., 2012. Locomotor head movements and
892 semicircular canal morphology in primates. Proc. Natl. Acad. Sci. USA 109, 17914–
893 17919.

894 Manoussaki, D., Dimitriadis, E.K., Chadwick, R.S., 2006. Cochlea's graded curvature
895 effect on low frequency waves. Phys. Rev. Lett. 96, 088701.
896 Mennecart, B., Costeur, L., 2016. Shape variation and ontogeny of the ruminant bony
897 labyrinth, an example in Tragulidae. J. Anat. 229, 422–435.
898 Mennecart, B., Rössner, G. E., Métais, G., DeMiguel, D., Schulz, G., Müller, B., Costeur,
899 L., 2016. The petrosal bone and bony labyrinth of early to middle Miocene European
900 deer (Mammalia, Cervidae) reveal their phylogeny. J. Morphol. 277, 1329–1338.
901 Mennecart, B., DeMiguel, D., Bibi, F., Rössner, G.E., Métais, G., Neenan, J.M., Wang, S.,
902 Schulz, G, Müller, B., Costeur, L., 2017. Bony labyrinth morphology clarifies the origin
903 and evolution of deer. Sci. Rep. 7, 13176.
904 Mitteroecker, P., Bookstein, F., 2011. Linear discrimination, ordination, and the
905 visualization of selection gradients in modern morphometrics. Evol. Biol. 38, 100–114.
906 Moyà-Solà, S., Köhler, M., 2000. Comprendere *Oreopithecus bambolii*, un ominoide
907 fossile enigmatico. Atti Mus. St. Nat. Maremma 18, 39–65.
908 Moyà-Solà, S., Köhler, M., Alba, D.M., 2001. *Egarapithecus narcisoi*, a new genus of
909 Pliopithecidae (Primates, Catarrhini) from the late Miocene of Spain. Am. J. Phys.
910 Anthropol. 114, 312–324.
911 Morimoto, N., Kunimatsu, Y., Nakatsukasa, M., Ponce de León, M. S., Zollikofer, C. P.,
912 Ishida, H., Sasaki, T., Suwa, G., 2020. Variation of bony labyrinthine morphology in
913 Mio–Plio–Pleistocene and modern anthropoids. Am. J. Phys. Anthropol. 173, 276–292.
914 Muller, M., Verhagen, J.H.G., 2002a. Optimization of the mechanical performance of a
915 two-duct semicircular duct system—Part 1: dynamics and duct dimensions. J. Theor.
916 Biol. 216, 409–424.
917 Muller, M., Verhagen, J.H.G., 2002b. Optimization of the mechanical performance of a
918 two-duct semicircular duct system—Part 2: excitation of endolymph movements. J.
919 Theor. Biol. 216, 425–442.

Muller, M., Verhagen, J.H.G., 2002c. Optimization of the mechanical performance of a two-duct semicircular duct system—Part 3: the positioning of the ducts in the head. J. Theor. Biol. 216, 443–459.

Nengo, I., Tafforeau, P., Gilbert, C.C., Fleagle, J.G., Miller, E.R., Feibel, C., Fox, D.L., Feinberg, J., Pugh, K.D., Berruyer, C., Mana, S., Engle, Z., Spoor, F., 2017. New infant cranium from the African Miocene sheds light on ape evolution. Nature 548, 169–174.

Pagel, M., 1999. Inferring the historical patterns of biological evolution. Nature 401, 877–884.

Perier, A., Lebrun, R., Marivaux, L., 2016. Different level of intraspecific variation of the bony labyrinth morphology in slow- versus fast-moving Primates. J. Mammal. Evol. 23, 353–368.

R Core Team, 2019. R: A language and environment for statistical computing. R Foundation for Statistical Computing, Vienna.

Rae, T.C., Johnson, P.M., Yano, W., Hirasaki, E. 2016. Semicircular canal size and locomotion in colobine monkeys: a cautionary tale. Folia Primatol. 87, 213–223.

Revell, L.J., 2012. Phytools: an R package for phylogenetic comparative biology (and other things). Methods Ecol. Evol. 3, 217–223.

Rook, L., Renne, P., Benvenuti, M., Papini, M., 2000. Geochronology of *Oreopithecus*-bearing succession at Baccinello (Italy) and the extinction pattern of european miocene hominoids. J. Hum. Evol. 39, 577–582.

Rook, L., Bondioli, L., Casali, F., Rossi, M., Köhler, M., Moyá Solá, S., Macchiarelli, R., 2004. The bony labyrinth of *Oreopithecus bambolii*. J. Hum. Evol. 46, 347–354.

Rose, M.D., 1994. Quadrupedalism in some Miocene catarrhines. J. Hum. Evol. 26, 387–411.

945 Russo, G.A., 2016. Comparative sacral morphology and the reconstructed tail lengths of
946 five extinct primates: *Proconsul heseloni*, *Epipliopithecus vindobonensis*,
947 *Archaeolemur edwardsi*, *Megaladapis grandidieri*, and *Palaeopropithecus kelyus*. J.
948 Hum. Evol. 90, 135–162.
949 Ryan, T.M., Silcox, M.T., Walker, A., Mao, X., Begun, D.R., Benefit, B.R., Gingerich, P.D.,
950 Köhler, M., Kordos, L., McCrossin, M.L., Moyà-Solà, S., Sanders, W.J., Seiffert, E.R.,
951 Simons, E., Zalmout, I.S., Spoor, F., 2012. Evolution of locomotion in Anthropoidea:
952 the semicircular canal evidence. P. Roy. Soc. B. 279, 3467–3475.
953 Sankhyan, A. R., Kelley, J., & Harrison, T. 2017. A highly derived pliopithecoid from the
954 Late Miocene of Haritalyangar, India. Journal of Human Evolution 105, 1–12.
955 Savje, F. 2019. distances: tools for distance metrics. https://cran.r-
956 project.org/web/packages/distances/index.html.
957 Schlager, S., 2017. Morpho and Rvcg – shape analysis in R: R-packages for geometric
958 morphometrics, shape analysis and surface manipulations. In: Zheng, G., Li, S.,
959 Székely, G. (Eds.), Statistical Shape and Deformation Analysis. Methods,
960 Implementation and Applications. Academic Press, London, pp. 217–256.
961 Seiffert, E.R., 2006. Revised age estimates for the later Paleogene mammal faunas of
962 Egypt and Oman. Proc. Natl. Acad. Sci. USA 103, 5000–5005.
963 Sidlauskas, B., 2008. Continuous and arrested morphological diversification in sister
964 clades of characiform fishes: a phylomorphospace approach. Evolution 62, 3135–
965 3156.
966 Silcox, M.T., Bloch, J.I., Boyer, D.M., Godinot, M., Ryan, T.M., Spoor, F., Walker, A., 2009.
967 Semicircular canal system in early primates. J. Hum. Evol. 56, 315–327.
968 Simons, E.L., Fleagle, J.G., 1973. The history of extinct gibbon-like primates. In:
969 Rumbaugh, D.M. (Ed.), Gibbon and Siamang Vol. 2. Anatomy, Dentition, Taxonomy,
970 Molecular Evolution and Behavior. Karger, Basel, pp. 121–148.

971 Simons, E.L., Seiffert, E.R., Ryan, T.M., Attia, Y., 2007. A remarkable female cranium of
972 the early Oligocene anthropoid *Aegyptopithecus zeuxis* (Catarrhini, Propliopithecidae).
973 Proc. Natl. Acad. Sci. USA 104, 8731–8736.
974 Spoor, F., Zonneveld., F., 1998. Comparative review of the human bony labyrinth. Yearb.
975 Phys. Anthropol. 41, 211–251.
976 Spoor, F., Garland, T., Krovitz, G., Ryan, T.M., Silcox, M.T., Walker, A., 2007. The primate
977 semicircular canal system and locomotion. Proc. Natl. Acad. Sci. USA 104, 10808–
978 10812.
979 Stevens, N.J., Seiffert, E.R., O'Connor, P.M., Roberts, E.M., Schmitz, M.D., Krause, C.,
980 Gorscak, E., Ngasala, S., Hieronymus, T.L., Temu, J., 2013. Palaeontological
981 evidence for an Oligocene divergence between Old World monkeys and apes. Nature
982 497, 611–614.
983 Swofford, D., 2003. PAUP*. Phylogenetic Analysis Using Parsimony (*and Other
984 Methods). Version 4. Sinauer Associates, Sunderland.
985 Szalay, F.S., 1975. Phylogeny of primate higher taxa: the basicranial evidence. In: Luckett,
986 W.P., Szalay, F.S. (Eds.), Phylogeny of the Primates: A Multidisciplinary Approach.
987 Plenum Press, New York, pp. 91–125.
988 Szalay, F.S., Delson, E., 1979. Evolutionary History of the Primates. Academic Press, New
989 York.
990 Tejedor, M.F., Rosenberger, A.L., 2008. A neotype for *Homunculus patagonicus*
991 Ameghino, 1891, and a new interpretation of the taxon. PaleoAnthropology 2008, 68–
992 82.
993 Urciuoli, A., Zanolli, C., Begun, D.R., Almécija, S., Dumoncel, J., Moyà-Solà, S., Alba,
994 D.M., 2019. A deformation-based geometric morphometric analysis of the vestibular
995 apparatus in the Miocene apes *Hispanopithecus laietanus* and *Rudapithecus*
996 *hungaricus*. Am. J. Phys. Anthropol. 168 (S68), 253.

997 Urciuoli, A., Zanolli, C., Beaudet, A., Dumoncel, J., Santos, F., Moyà-Solà, S., Alba, D.M.,
998 2020. The evolution of the vestibular apparatus in apes and humans. eLife 9, e51261.
999 van der Meulen, A.J., García-Paredes, I., Álvarez-Sierra, M.Á., van den Hoek Ostende,
1000 L.W., Hordijk, K., Oliver, A., López-Guerrero, P., Hernández-Ballarín, V., Peláez-
1001 Campomanes, P., 2011. Biostratigraphy or biochronology? Lessons from the Early
1002 and Middle Miocene small Mammal Events in Europe. Geobios 44, 309–321.
1003 Zalmout, I.S., Sanders, W.J., MacLatchy, L., Gunnell, G., Al-Mufarreh, Y.A., Ali, M.A.,
1004 Nasser, A.-A. H., Al-Masary, A.M., Al-Sobhi, S.A., Nadhra, A.O., Matari, A.H., Wilson,
1005 J. A., Gingerich, P. D., 2010. New Oligocene primate from Saudi Arabia and the
1006 divergence of apes and Old World monkeys. Nature 466, 360–365.
1007 Zapfe, H., 1958. The skeleton of *Pliopithecus* (*Epipliopithecus*) *vindobonensis* Zapfe and
1008 Hürzeler. Am. J. Phys. Anthropol. 16, 441–457.
1009 Zapfe, H., 1961. Die Primatenfunde aus der miozänen Spaltenfüllung von Neudorf an der
1010 March (Děvínská Nová Ves), Tschechoslowakei. Schweizer. palaeontol. Abh. 78, 1–
1011 293.
1012 Zapfe, H., Hürzeler, J., 1957. Die Fauna der miozänen Spaltenfüllung von Neudorf an der
1013 March (ČSR.). Primates. Sitzungsber. Öst. Akad. Wiss. Math. Naturwiss. Kl. 166, 113–
1014 123.
1015

1016 **Figure captions**

1017

1018 **Figure 1.** Illustration of the protocol used for digitally separating the cochlea (green) from
1019 the semicircular canals and the vestibule (blue). a) In anterior view, the first landmark
1020 (yellow filled circle) is placed anteriorly to the oval window, on the point of maximum
1021 surface curvature of the ridge-like morphology formed by the narrowing of the vestibule. b)
1022 In posterior view, three landmarks are placed along the junction between the bony

vestibule and the cochlea, defined by the line of maximum surface curvature found immediately below the bulge formed by the saccular recess. A cutting plane (here perpendicular to the view and depicted by a black line) is best fitted to the identified landmarks using the 'Points To Fit' option of the 'Clipping Plane' module of Avizo version 9.0.1 (FEI Visualization Sciences Group, Houston) via a customized script (available upon request to A.U.), and used as a reference for a straight cut. Abbreviations: asc = anterior semicircular canal; psc = posterior semicircular canal; lsc = lateral semicircular canal; CC = common crus.

Figure 2. Cladogram of extant and fossil anthropoids showing the two phylogenetic hypotheses for *Epipliopithecus*. The solid line (A) denotes the most widely accepted phylogenetic position of *Epipliopithecus* as a stem catarrhine, whereas the dashed line (B) denotes the alternative hypothesis that *Epipliopithecus* would be more closely related to hominoids. Key nodes are highlighted as follows: gray circle = crown anthropoids; green circle = crown platyrrhines; blue circle = crown catarrhines; orange circle = crown hominoids. Skulls and crania (not to scale) were taken from the following sources for illustrative purposes only: extant skulls and *Aegyptopithecus*, Wikimedia Commons; *Dolichocebus*, Kay et al. (2009b: Fig. 1); *Homunculus*, Tejedor and Rosenberger (2008: Fig. 2); *Oreopithecus* (reconstruction), Moyà-Solà and Köhler (2000: Fig. 5); *Epipliopithecus*, photograph of a cast; *Parapithecus*, digital reconstruction with photographic texture made by Steven Heritage.

Figure 3. Phylogenetic trees used for the phylomorphospace approach. They differ in considering *Epipliopithecus* as a stem catarrhine (a) or a stem hominoid (b).

Figure 4. Rendered 3D models of the semicircular canals and vestibule of *Epipliopithecus vindobonensis* (all specimens depicted as from the left side) and selected extant anthropoids, in lateral (left), superior (middle), and posterior (right) views: a) *E. vindobonensis* (individual II, NHMW 1970/1397/0003, mirrored); b) *E. vindobonensis* (individual III, NMB OE 303a); c) *E. vindobonensis* (individual III, NMB OE 303b, mirrored); d) *Parapithecus grangeri* (DPC 18651); e) *Dolichocebus gaimanensis* (MACN 14128); f) *Homunculus patagonicus* (MPM-PV 3501); g) *Ateles geoffroyi* (MCZ 29628); h) *Alouatta palliata* (DU EA LP12); i) *Cebus apella* (MCZ27891); j) *Aegyptopithecus zeuxis* (CGM 85785); k) *Trachypithecus cristatus* (MCZ35603); l) *Chlorocebus pygerythrus* (SIU 4796); m) *Macaca fascicularis* (MCZ 35765); n) *Oreopithecus bambolii* (BAC 208); o) *Hylobates lar* (MCZ 41424); p) *Symphalangus syndactylus* (AMNH.M 106583); q) *Hoolock hoolock* (AMNH.M 83425); r) *Pongo pygmaeus* (IPS10647); s) *Gorilla gorilla* (AMNH.M 167338; t) *Pan paniscus* (MCZ 38019); u) *Homo sapiens* (EMBR 179). Scale bars equal 5 mm.

Figure 5. Bivariate plot of canal log-transformed cube root canal volume (mm; Ln VolSC) vs. log-transformed canal length (mm; ln L). Separate regression lines are depicted for hominids (red line) and for nonhominid anthropoids (blue line). *Epipliopithecus* (NHMW 1970/1397/0003 and NMB OE 303a, b) falls within the variability of nonhominid anthropoids, similar to all extinct taxa except *Oreopithecus*. Measurements for the included fossil taxa given in Table 6.

Figure 6. Patterns of vestibule and semicircular canal shape variation among major anthropoid clades based on the results of a between-group principal component analysis, as depicted by bivariate plots between principal components (bgPCs): a) bgPC2 vs. bgPC1; b) bgPC3 vs. bgPC1. Variance explained by each component is given along each axis. c–e) Extreme conformations of maximum (above) and minimum (below) bgPC

scores: c) bgPC1; d) bgPC2; e) bgPC3. Four groups (platyrrhines, cercopithecoids, hylobatids, and hominids) were defined a priori, whereas specimens of *Epipliopithecus vindobonensis* were plotted post hoc onto the morphospace. Renderings in lateral (left), superior (middle), and posterior (right) views of warped 3D models representing the extreme conformations for each bgPC are placed close to the corresponding axis. Convex hulls depict the range of variation for a priori defined groups using the following color code: green = platyrrhines; blue = cercopithecoids; red = hylobatids; orange = hominids.

Figure 7. Dendrogram resulting from a cluster analysis (Ward's method) based on Mahalanobis distances computed between the species centroids of the between-group principal component analysis (bgPCA) of shape data. The cophenetic correlation coefficient is 0.703.

Figure 8. Phylomorphospace of the anthropoid semicircular canal. The phylogenetic tree (with *Epipliopithecus* included as a stem catarrhine; Fig. 3a) is projected onto the tangent space defined by the between-group principal components (bgPCs) as depicted in Figure 6. The internal nodes (i.e., the ancestral states) were estimated using maximum likelihood: a) bgPC2 vs. bgPC1; b) bgPC3 vs. bgPC1. Variance explained by each component is given along each axis. Convex hulls depict the range of variation for a priori defined groups using the following color code: green = platyrrhines; blue = cercopithecoids; red = hylobatids; orange = hominids. The ancestral nodes discussed for assessing *Epipliopithecus* phylogenetic affinities do not change consistently in their position in the morphospace irrespective of the phylogenetic hypothesis used for their estimation (see SOM Fig. S3 for the alternative phylogenetic tree including *Epipliopithecus* as a stem hominoid). Key nodes are highlighted as follows: gray circle = crown anthropoids; green

1099 circle = crown platyrrhines; blue circle = crown catarrhines; orange circle = crown
1100 hominoids.
1101
1102 **Figure 9.** Reconstruction of the semicircular canals and vestibule for the last common
1103 ancestors (LCAs) of the following clades: a) crown anthropoids; b) crown platyrrhines; c)
1104 crown catarrhines; d) crown hominoids. The renderings of each 3D model are depicted in
1105 lateral (left), superior (middle), and posterior (right) views.
1106
1107 **Figure 10.** Box-and-whisker plot of allometric residuals based on best-fit line of the
1108 nonhominid anthropoid regression of log-transformed cube root of canal volume and log-
1109 transformed canal length (as depicted in Fig. 5). Vertical lines correspond to the median,
1110 boxes depict interquartile range, whiskers represent maximum and minimum values within
1111 1.5 times the interquartile range, and black dots are outliers. Sample sizes for extant
1112 groups are the following: Platyrrhini (*n* = 40), Cercopithecoidea (*n* = 75), Hylobatidae (*n* =
1113 17), Hominidae (*n* = 30).
1114
1115 **Figure 11.** Illustration of the discrete characters of semicircular canal (SC) and vestibule
1116 morphology used in this paper. Numbers preceding each state (0, 1, 2) correspond to
1117 character states numbered in Tables 8 and 9, and SOM Table S4.
1118
1119 **Figure 12.** Simplified cladogram of crown anthropoids and selected extinct catarrhines
1120 (*Epipliopithecus* and *Oreopithecus*) summarizing the main synapomorphies inferred for the
1121 various clades in semicircular canal and vestibule morphology. The four extant anthropoid
1122 clades distinguished (platyrrhines, cercopithecoids, hylobatids and hominids) are depicted
1123 as terminal nodes. The synapomorphies inferred for each node are summarized below;
1124 character number (preceded by a hash) and character state (within parentheses) are

provided after each synapomorphy within brackets. a) *Epipliopithecus* + crown catarrhines: rounded anterior canal [#3(1)]; b) Crown catarrhines: rounded posterior canal [#5(1)], moderately short CC [#7(1)]; c) *Oreopithecus* + crown hominoids: vertically compressed anterior canal [#3(0)], anterosuperiorly-projecting anterior portion of the anterior canal [#4(1)], short CC [#7(2)]; d) Crown hominoids: markedly superiorly bent ampullary portion of the lateral canal [#6(1)]; e) Crown hominids (unless *Oreopithecus* + crown hominoid synapomorphies [node c] with reversal in hylobatids): large vestibule relative to the SCs [#1(1)], stout SCs [#2(1)]. Abbreviations: CC = common crus; SC = semicircular canals. See Figure 11 for an illustration of the various character states and Table 9 and SOM Table S4 for the scoring of reconstructed last common ancestors and individual taxa, respectively.

Figure 1

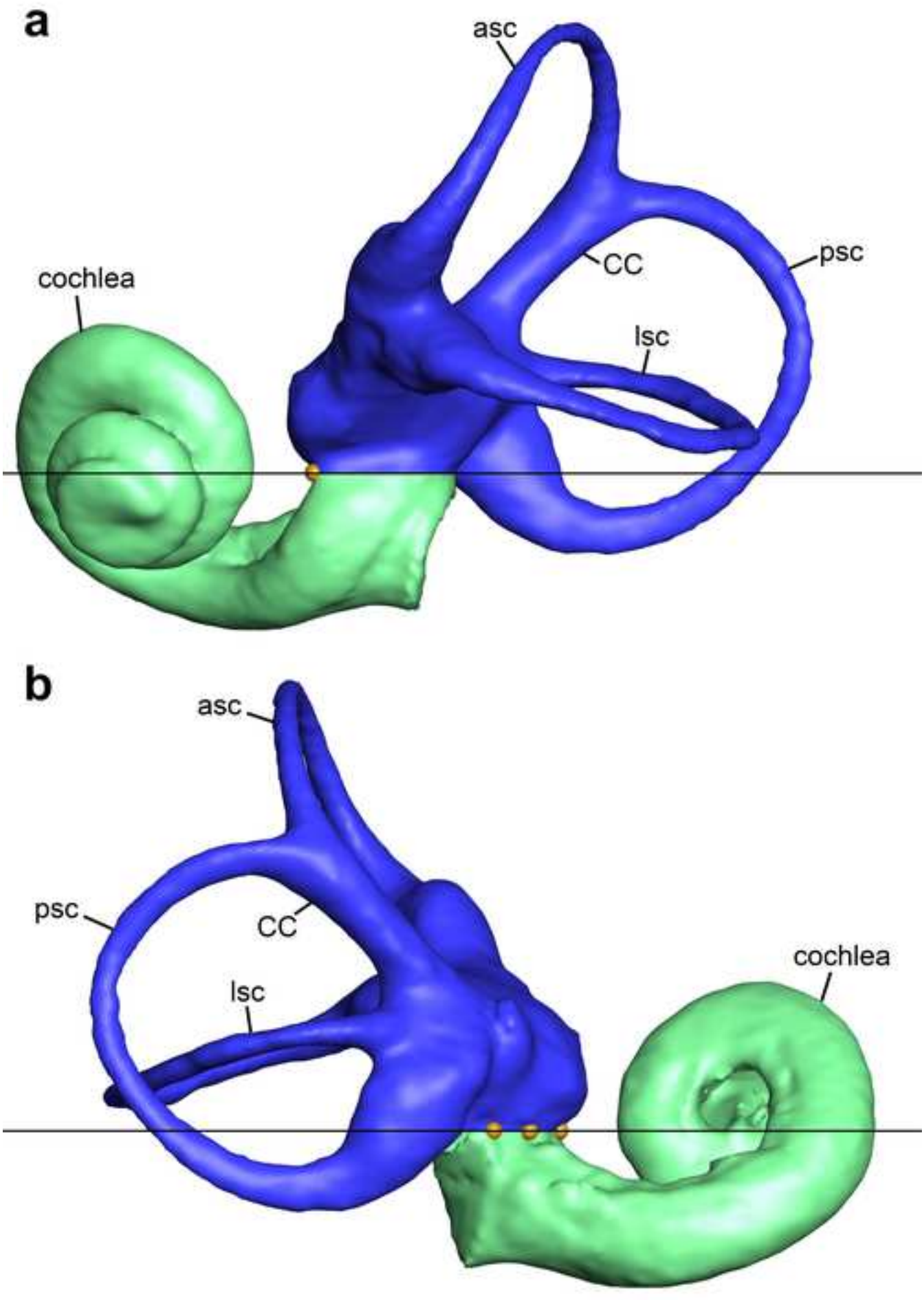

Figure 2

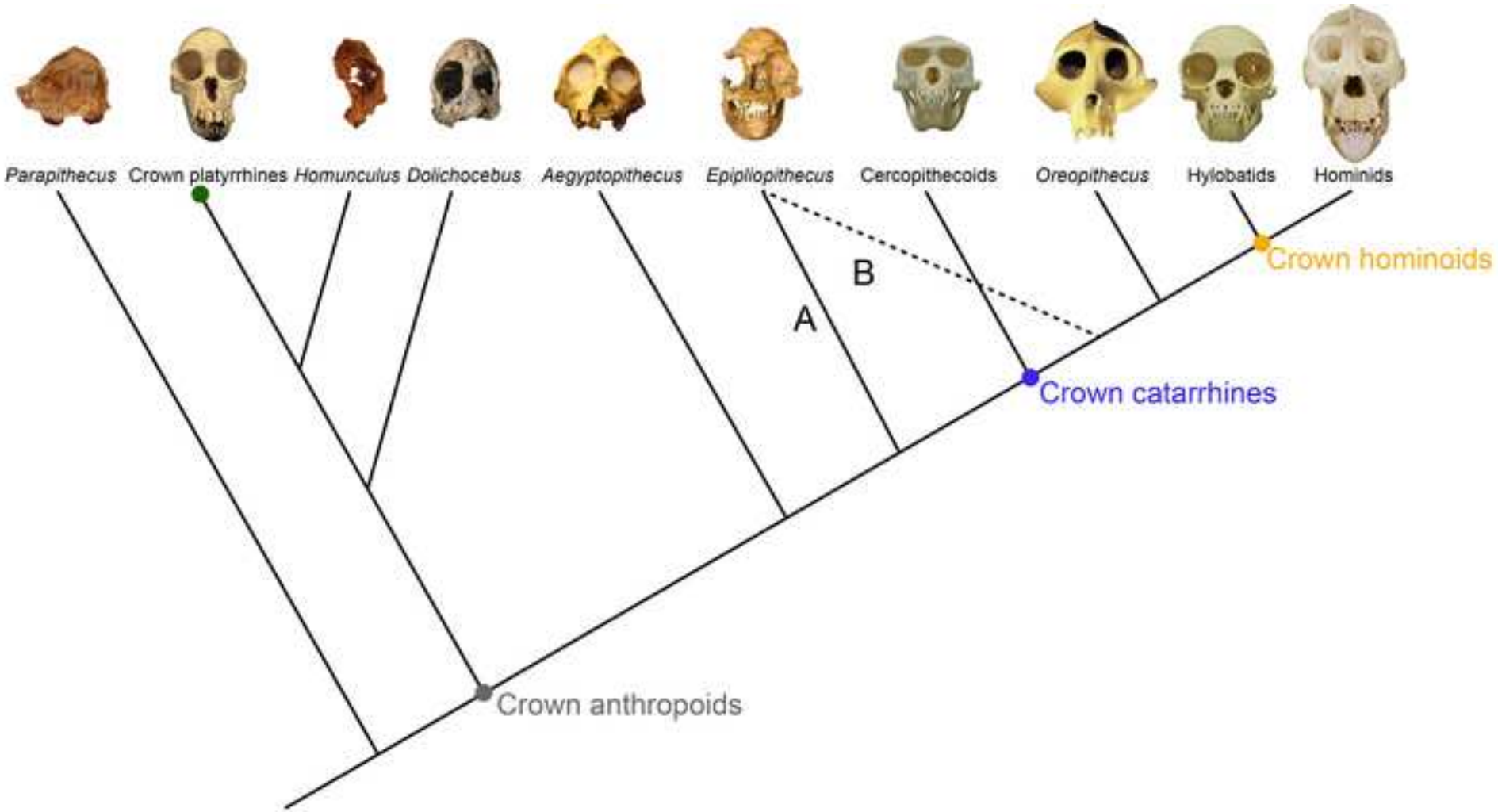

Figure 3

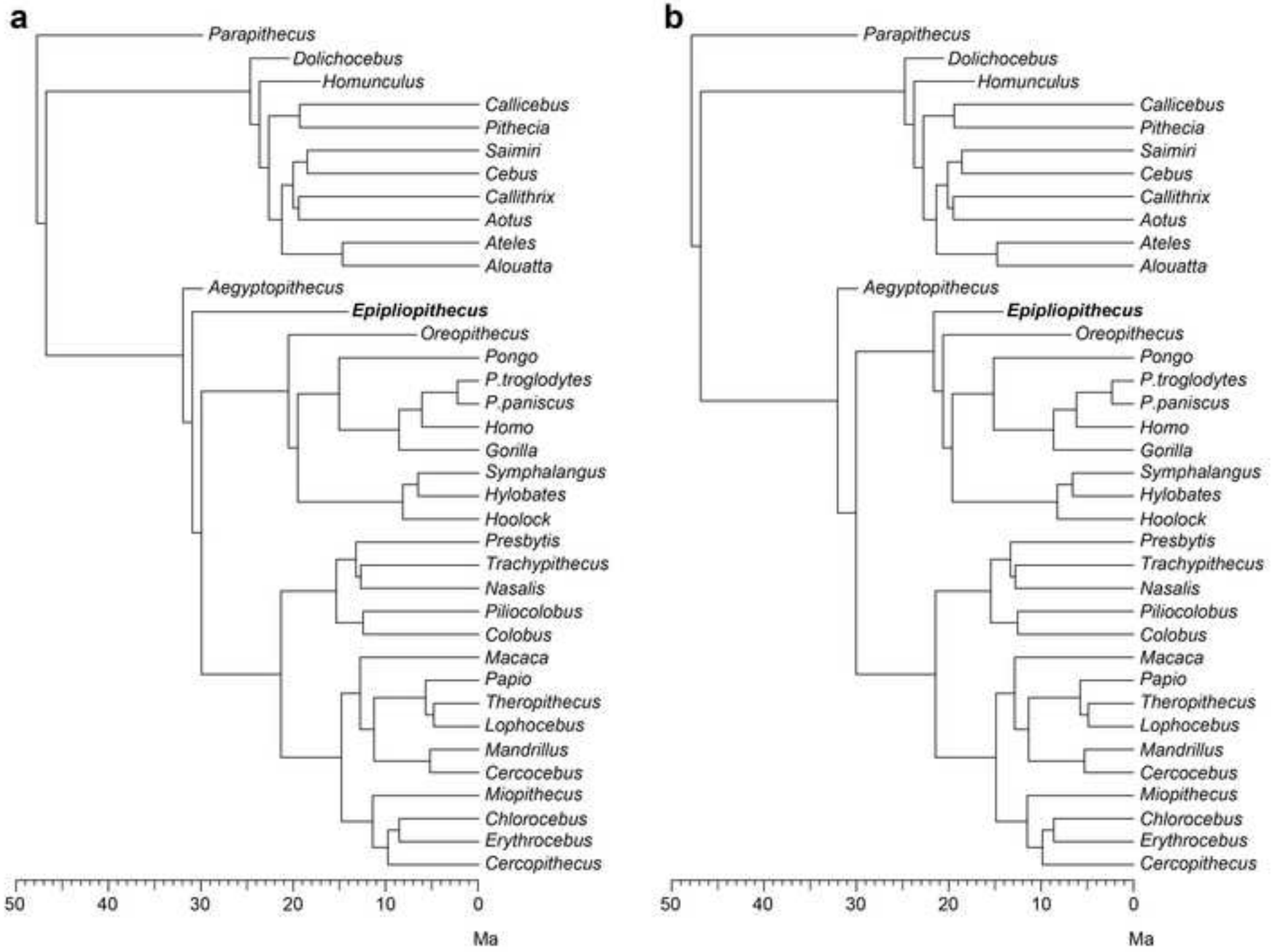

Figure 4

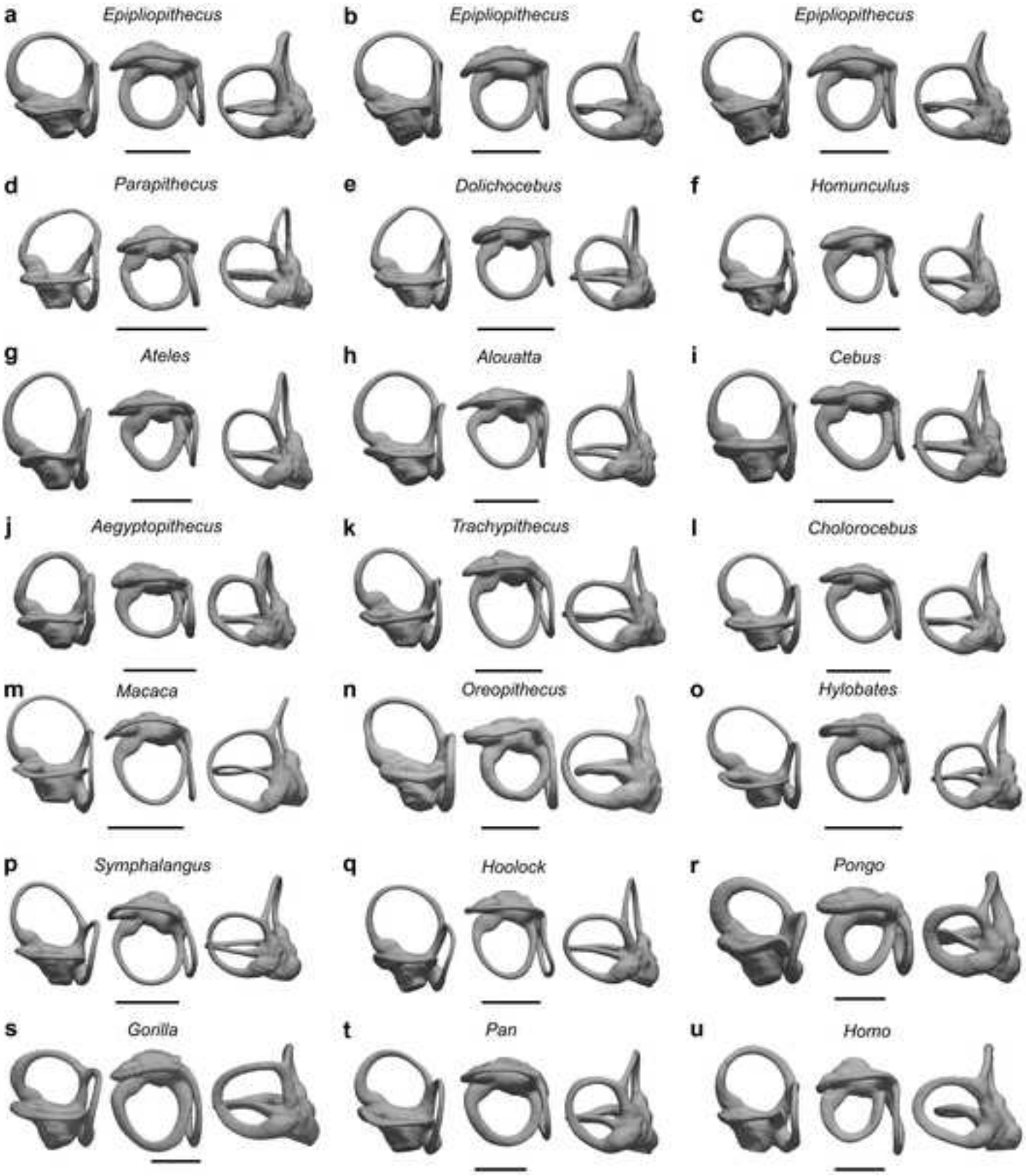

Figure 5

Click here to access/download;Figure;Figure_5.tif

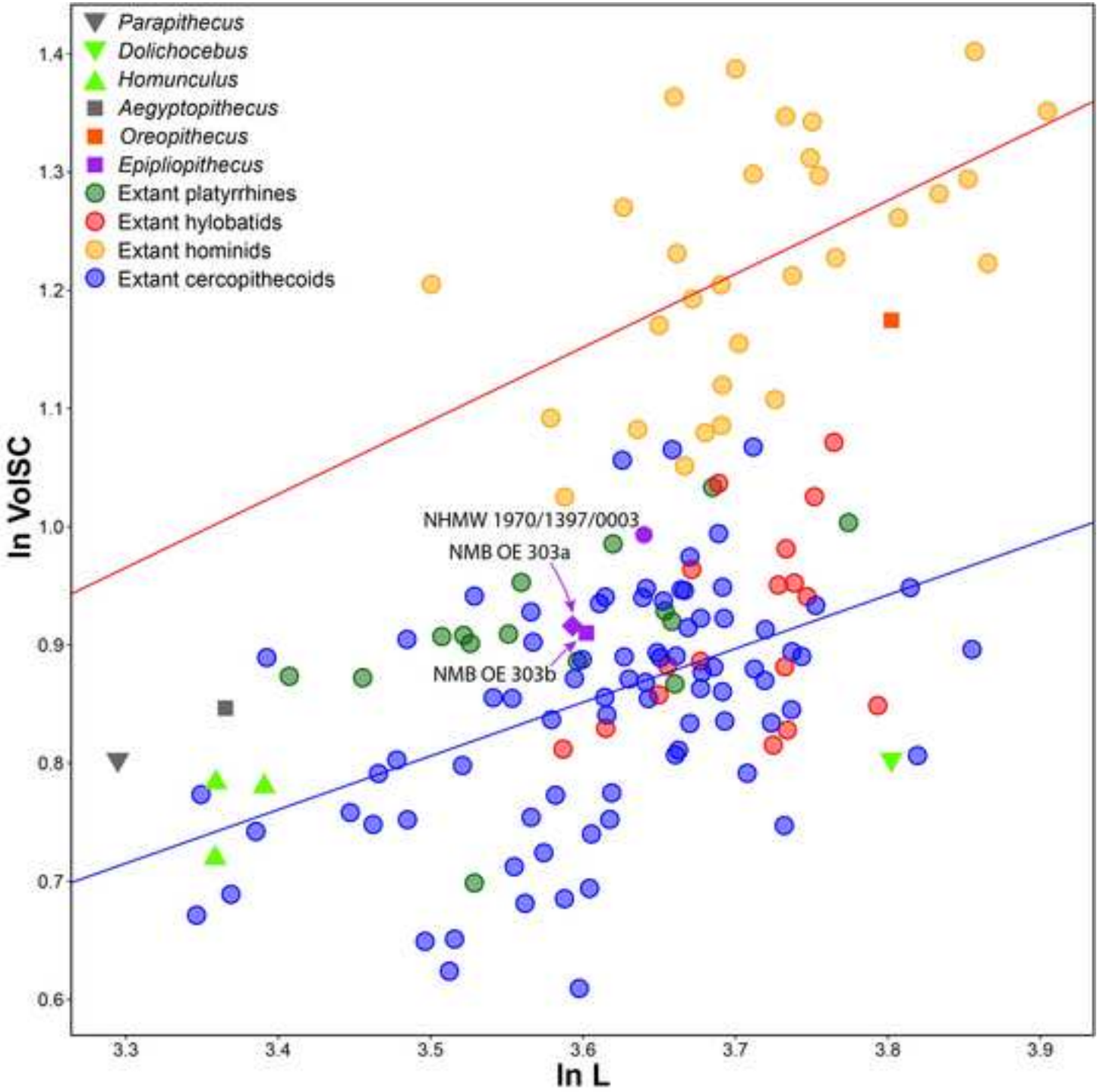

Figure 6

Click here to access/download;Figure;Figure_6.tif

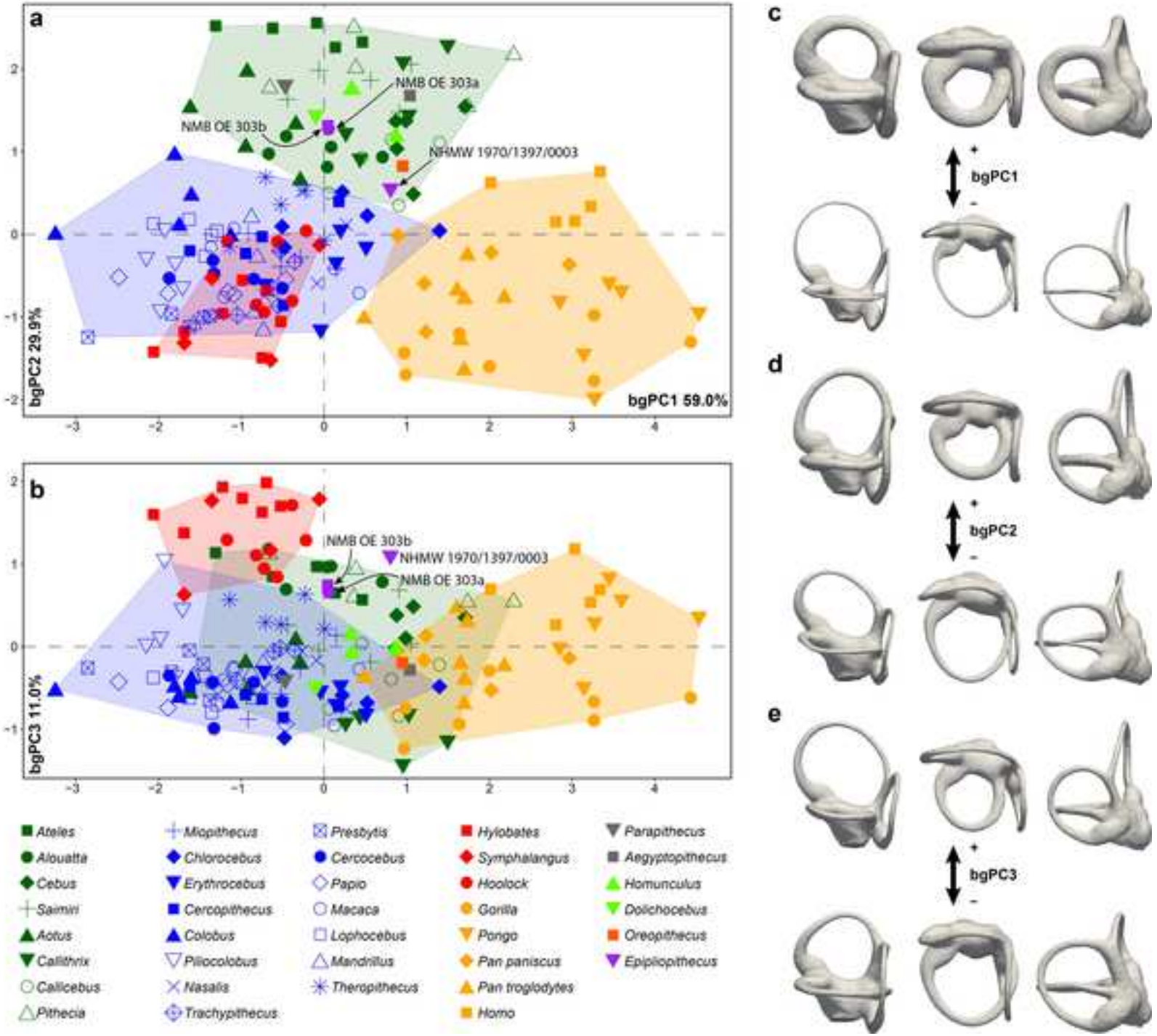

Figure 7

Click here to access/download;Figure;Figure_7.tif

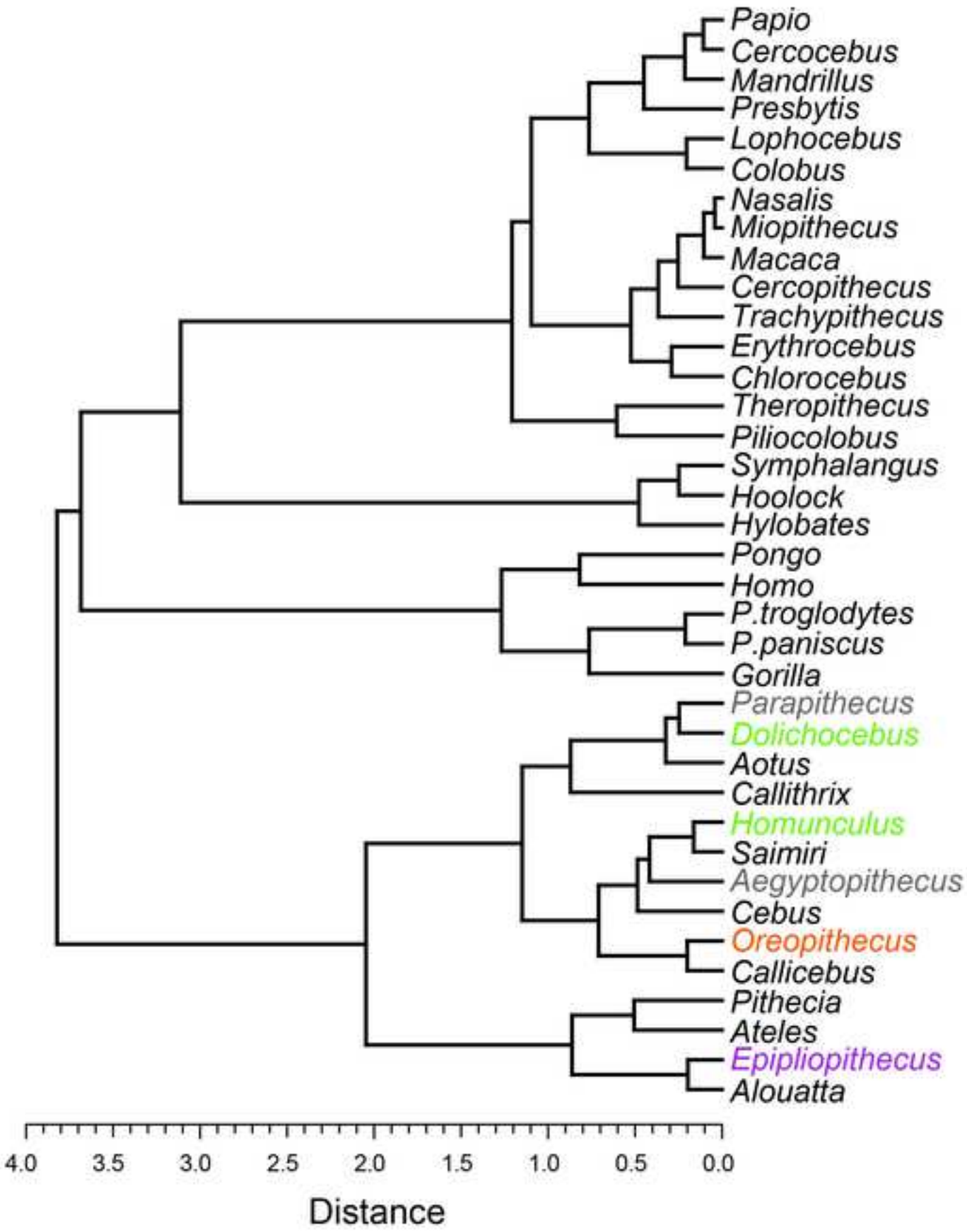

Figure 8

Click here to access/download;Figure;Figure_8.tif

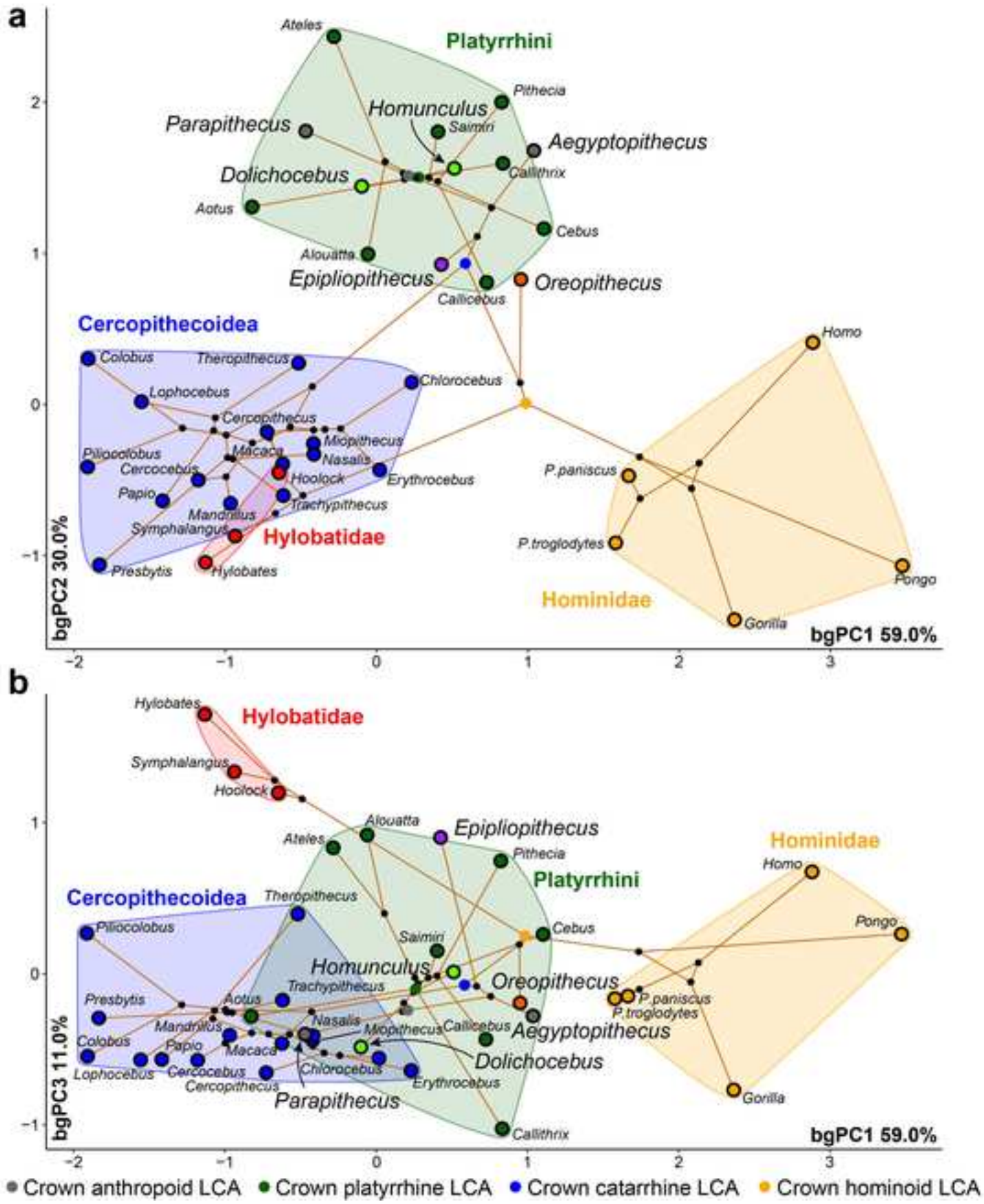

Figure 9

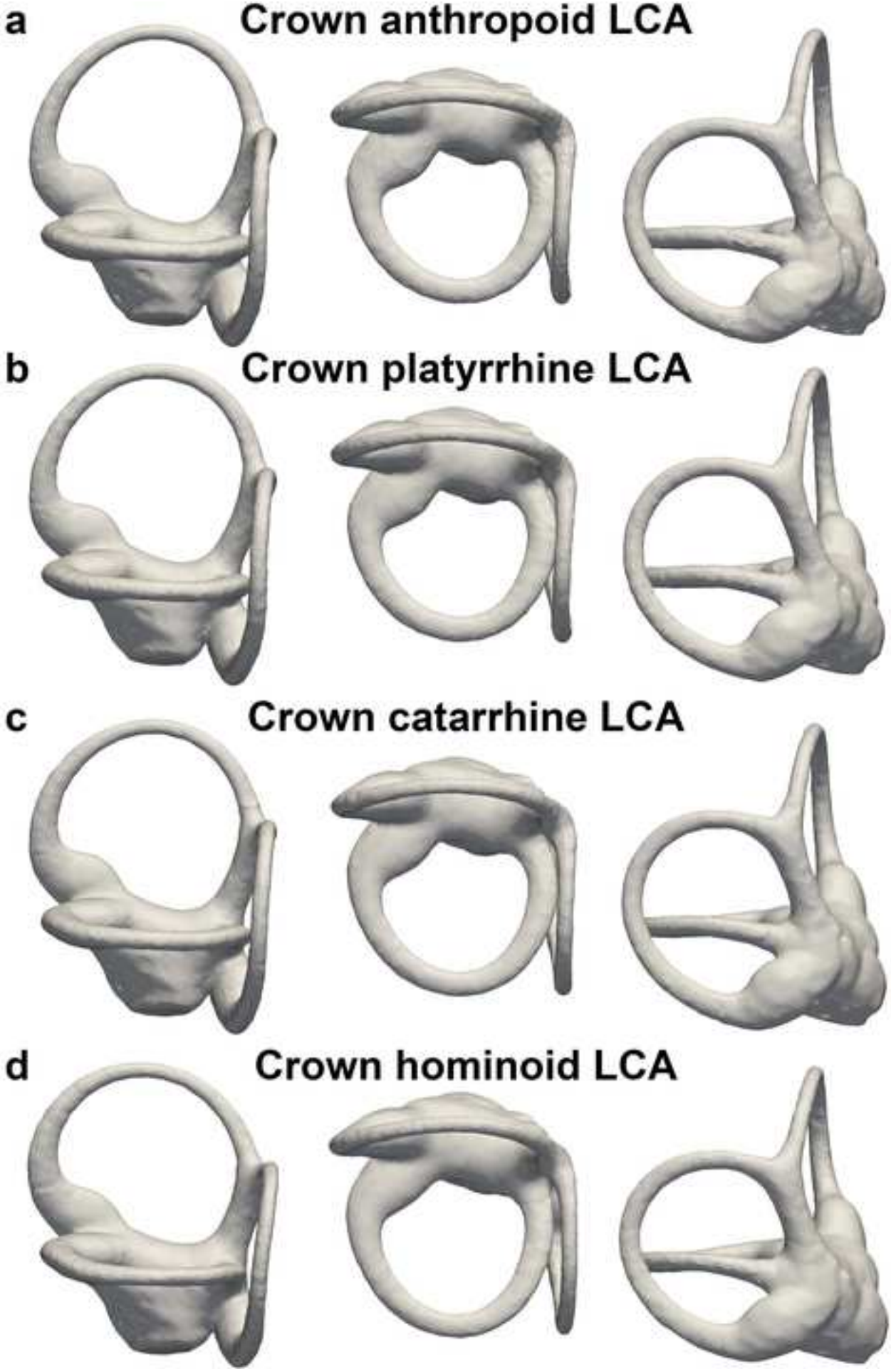

Figure 10

Click here to access/download;Figure;Figure_10.tif

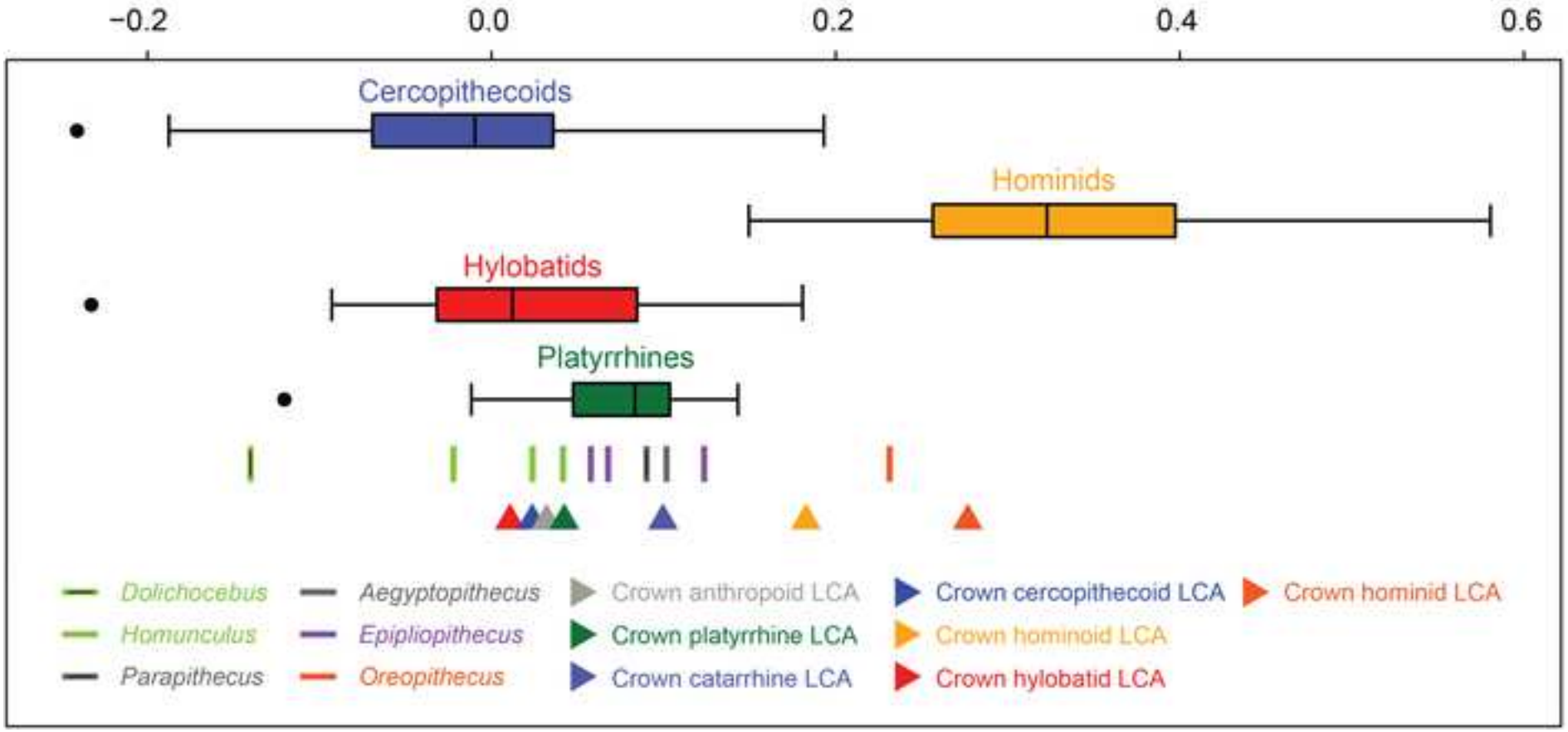

Figure 11

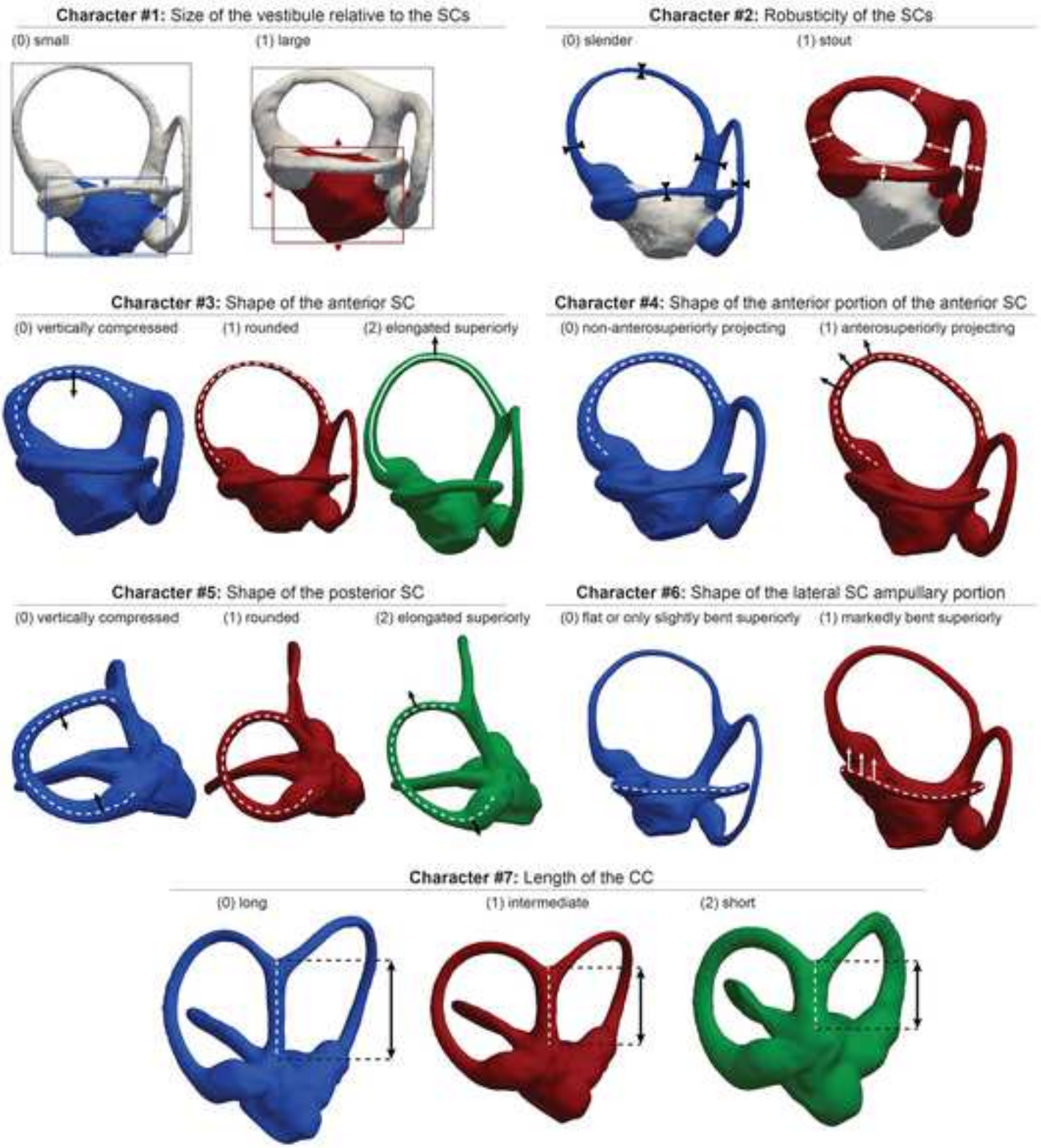

Figure 12

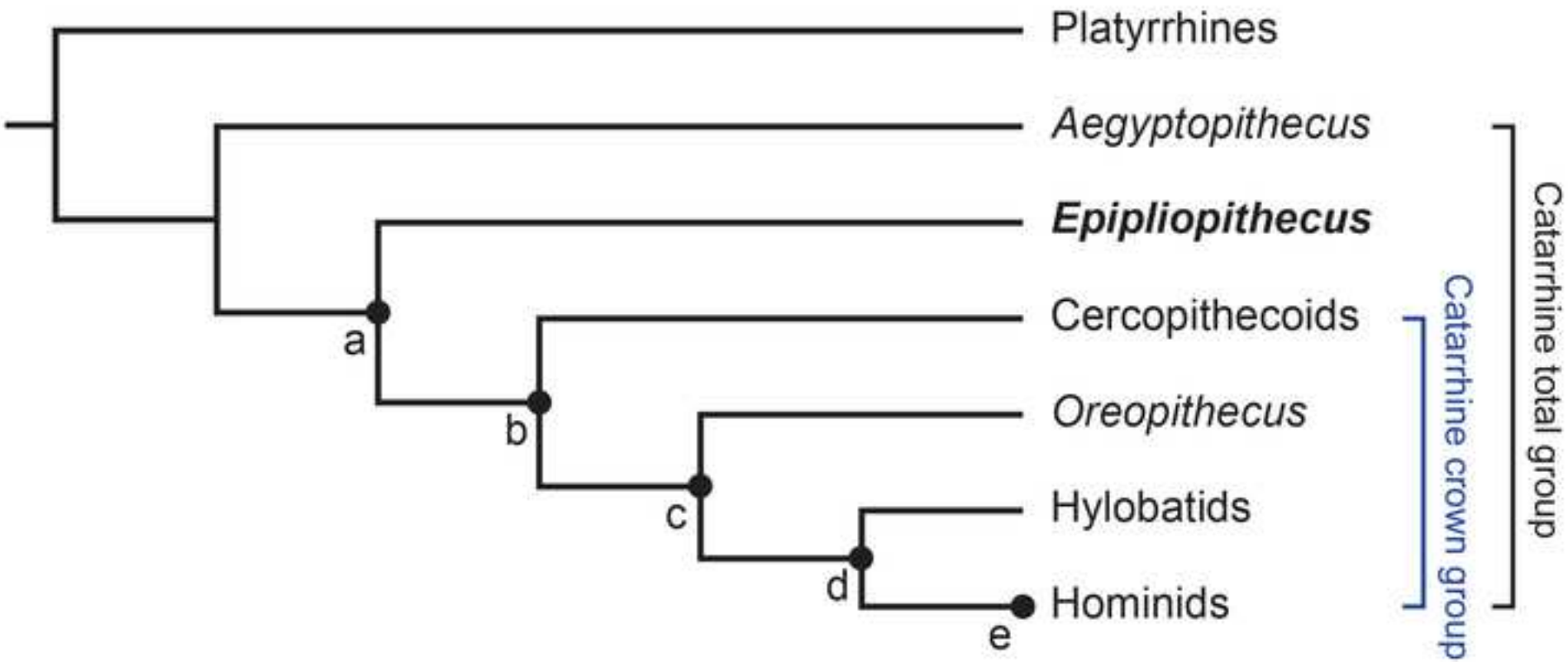

Table 1

Digital object identifiers (DOIs) of the 3D virtual models of the vestibule and semicircular canals of *Epipliopithecus vindobonensis* available from MorphoSource.org. (https://www.morphosource.org).

Catalog No.	Museum	DOI
NMBOE 303a (individual III)	NMBOE	https://doi.org/10.17602/M2/M113935
NMBOE 303b (individual III)	NMBOE	https://doi.org/10.17602/M2/M113933
NHMW 1970/1397/0003 (individual II)	NHMW	https://doi.org/10.17602/M2/M113932

Abbreviations: NMB OE = Naturhistorisches Museum Basel, Switzerland; NHMW, Naturhistorisches Museum Wien, Austria.

Table 2

Log-transformed cube root of canal volume (ln VolSC, mm^3) and log-transformed canal length (ln L, mm) measured for the fossil taxa included in the analysis.[a]

Catalog No.	Taxon	ln VolSC	ln L
NMBOE 303a	*Epipliopithecus vindobonensis*	3.640	0.993
NMBOE 303b	*Epipliopithecus vindobonensis*	3.602	0.910
NHMW 1970/1397/0003	*Epipliopithecus vindobonensis*	3.593	0.916
CGM 85785	*Aegyptopithecus zeuxis*	3.365	0.847
MPM-PV 30501	*Homunculus patagonicus*	3.391	0.780
MPM-PV 30502	*Homunculus patagonicus*	3.359	0.720
MPM-PV 30503	*Homunculus patagonicus*	3.359	0.784
MACN 14128	*Dolichocebus gaimanensis*	3.802	0.803
BAC 208	*Oreopithecus bambolii*	3.295	0.803
DPC 18651	*Parapithecus grangeri*	3.640	0.993

Abbreviations: BAC = Baccinello (field acronym; housed at Naturhistorisches Museum Basel, Switzerland); CGM = Egyptian Geological Museum, Cairo, Egypt; MPM-PV = Museo Regional Provincial Padre M.J. Molina, Río Gallegos, Argentina; MACN = Museo Argentino de Ciencias Naturales, Buenos Aires, Argentina; DPC = Duke Lemur Center, Durham, NC, USA.

[a] See SOM Table S1 for the specimens included in the extant comparative sample.

Table 3

Mahalanobis distances (D^2) and posterior probabilities of group membership (*p*) based on the scores for fossil specimens in the between-group principal component analysis for the entire anthropoid sample.[a-b]

D^2	Cercopithecoidea	Hominidae	Hylobatidae	Platyrrhini
Epipliopithecus vindobonensis (NHMW 1970/1397/0003)	17.179	10.539	6.485	**3.437**
Epipliopithecus vindobonensis (NMB OE 303a)	12.190	14.262	6.588	**0.779**
Epipliopithecus vindobonensis (NMB OE 303b)	13.307	15.085	6.682	**1.056**
Oreopithecus bambolii (BAC 208)	8.083	5.450	11.574	**1.579**
Aegyptopithecus zeuxis (CGM 85785)	12.430	9.133	15.513	**0.990**
Homunculus patagonicus (MPM-PV 3501)	11.817	13.356	11.017	**0.073**
Homunculus patagonicus (MPM-PV 3502)	10.336	12.736	12.056	**0.165**
Homunculus patagonicus (MPM-PV 3503)	10.083	7.449	11.284	**0.590**
Dolichocebus gaimanensis (MACN 14128)	5.204	13.516	12.687	**1.935**
Parapithecus grangeri (DPC 18651)	6.533	17.859	13.047	**2.110**
p	Cercopithecoidea	Hominidae	Hylobatidae	Platyrrhini
Epipliopithecus vindobonensis (NHMW 1970/1397/0003)	0.006	0.007	0.018	**0.029**
Epipliopithecus vindobonensis (NMB OE 303a)	0.018	<0.001	<0.001	**0.678**

Epipliopithecus vindobonensis (NMB OE 303b)	0.013	<0.001	<0.001	**0.608**
Oreopithecus bambolii (BAC 208)	0.052	0.005	<0.001	**0.530**
Aegyptopithecus zeuxis (CGM 85785)	0.001	<0.001	<0.001	**0.688**
Homunculus patagonicus (MPM-PV 3501)	0.003	<0.001	<0.001	**0.980**
Homunculus patagonicus (MPM-PV 3502)	0.003	<0.001	<0.001	**0.919**
Homunculus patagonicus (MPM-PV 3503)	0.019	0.001	<0.001	**0.848**
Dolichocebus gaimanensis (MACN 14128)	0.013	<0.001	<0.001	**0.612**
Parapithecus grangeri (DPC 18651)	0.002	<0.001	<0.001	**0.411**

Abbreviations: NHMW = Naturhistorisches Museum of Wien, Austria; NMB = Naturhistorisches Museum of Basel, Switzerland; BAC = NMB accession number for *Oreopithecus bambolii* specimens; CGM = Egyptian Geological Museum, Cairo, Egypt; MPM-PV = Museo Regional Provincial "Padre M.J. Molina", Río Gallegos, Argentina; MACN = Museo Argentino de Ciencias Naturales, Buenos Aires, Argentina; DPC = Duke Lemur Center, Durham, NC, USA.

[a] Note that these are probability estimates of having a particular score given membership in a particular group, not the likelihood of group membership in each of the a priori defined groups given a particular score (the greater the number, the higher the probability).

[b] The lowest distance (D^2) and highest posterior probability of group membership (*p*) for each specimen are bolded.

Table 4

Mahalanobis distances (D^2) and posterior probabilities of group membership (*p*) based on the scores for fossil specimens in the between-group principal component analysis for the entire anthropoid sample and considering all catarrhines as a single group.[a-b]

D^2	Catarrhini	Platyrrhini
Epipliopithecus vindobonensis (NHMW 1970/1397/0003)	13.016	**5.341**
Epipliopithecus vindobonensis (NMB OE 303a)	11.837	**1.654**
Epipliopithecus vindobonensis (NMB OE 303b)	13.040	**2.098**
Oreopithecus bambolii (BAC 208)	9.085	**3.890**
Aegyptopithecus zeuxis (CGM 85785)	16.900	**3.204**
Homunculus patagonicus (MPM-PV 3501)	13.814	**0.135**
Homunculus patagonicus (MPM-PV 3502)	13.057	**0.284**
Homunculus patagonicus (MPM-PV 3503)	10.989	**1.806**
Dolichocebus gaimanensis (MACN 14128)	8.645	**2.417**
Parapithecus grangeri (DPC 18651)	12.592	**3.670**
p	Catarrhini	Platyrrhini
Epipliopithecus vindobonensis (NHMW 1970/1397/0003)	0.109	**0.241**
Epipliopithecus vindobonensis (NMB OE 303a)	0.022	**0.876**
Epipliopithecus vindobonensis (NMB OE 303b)	0.017	**0.847**
Oreopithecus bambolii (BAC 208)	0.124	**0.673**
Aegyptopithecus zeuxis (CGM 85785)	0.002	**0.886**
Homunculus patagonicus (MPM-PV 3501)	0.002	**0.985**
Homunculus patagonicus (MPM-PV 3502)	0.002	**0.968**
Homunculus patagonicus (MPM-PV 3503)	0.034	**0.935**

Dolichocebus gaimanensis (MACN 14128)	0.013	**0.841**
Parapithecus grangeri (DPC 18651)	0.002	**0.795**

Abbreviations: NHMW = Naturhistorisches Museum of Wien, Austria; NMB = Naturhistorisches Museum of Basel, Switzerland; BAC = NMB accession number for *Oreopithecus bambolii* specimens; CGM = Egyptian Geological Museum, Cairo, Egypt; MPM-PV = Museo Regional Provincial "Padre M.J. Molina", Río Gallegos, Argentina; MACN = Museo Argentino de Ciencias Naturales, Buenos Aires, Argentina; DPC = Duke Lemur Center, Durham, NC, USA.

[a] Note that these are probability estimates of having a particular score given membership in a particular group, not the likelihood of group membership in each of the a priori defined groups given a particular score (the greater the number, the higher the probability).

[b] The lowest distance and highest probability for each specimen are bolded.

Table 5

Mahalanobis distances (D^2) between specimens of *Epipliopithecus* and other fossils based on between group principal component analysis scores.

D^2	NHMW 1970/1397/0003	NMB OE 303a	NMB OE 303b
Epipliopithecus vindobonensis (NHMW 1970/1397/0003)	—	1.332	1.285
Epipliopithecus vindobonensis (NMB OE 303a)	1.332	—	0.176
Epipliopithecus vindobonensis (NMB OE 303b)	1.285	0.176	—
Oreopithecus bambolii (BAC 208)	2.244	1.901	2.055
Aegyptopithecus zeuxis (CGM 85785)	2.360	1.804	1.927
Homunculus patagonicus (MPM-PV 3501)	1.943	0.919	1.033
Homunculus patagonicus (MPM-PV 3502)	2.246	1.251	1.388
Homunculus patagonicus (MPM-PV 3503)	1.914	1.450	1.592
Dolichocebus gaimanensis (MACN 14128)	3.081	2.077	2.243
Parapithecus grangeri (DPC18651)	3.201	2.017	2.161

Abbreviations: NHMW = Naturhistorisches Museum Wien, Austria; NMB OE = Naturhistorisches Museum Basel, Switzerland; BAC = Baccinello (housed at NMB); CGM = Egyptian Geological Museum, Cairo, Egypt; MPM-PV = Museo Regional Provincial Padre

M.J. Molina, Río Gallegos, Argentina; MACN = Museo Argentino de Ciencias Naturales, Buenos Aires, Argentina; DPC = Duke Lemur Center, Durham, NC, USA.

Table 6

Phylogenetic signal computed for the between-group principal analysis applied to the deformation fields of the extant anthropoid comparative sample. The variance explained by each principal component (bgPC) and the *p*-value for the statistics are given within parentheses.

	bgPC1 (59%)	bgPC2 (30%)	bgPC3 (11%)
Pagel's λ	1.000 ($p < 0.0001$)	0.843 ($p < 0.0001$)	0.925 ($p < 0.0001$)
Blomberg's K	1.148 ($p < 0.0001$)	1.446 ($p < 0.001$)	0.732 ($p < 0.001$)

Table 7

Weighted Euclidean distances computed between the between-group principal component scores of the reconstructed last common ancestors (LCAs) and the *Epipliopithecus* centroid.

LCA	Distance
Crown anthropoids	1.304
Crown platyrrhines	1.141
Crown catarrhines	0.989
Crown cercopithecoids	1.646
Crown hominoids	1.256

Table 8

Definition of the discrete characters of semicircular canal (SC) and vestibule morphology used in this paper**.**

Character No.	Character statements (characters + character states)
#1	Size of the vestibule relative to the SCs: 0 = small; 1 = large.
#2	Robusticity of the SCs: 0 = slender; 1 = stout.
#3	Shape of the anterior SC: 0 = vertically compressed; 1 = rounded; 2 = elongated superiorly.
#4	Shape of the anterior portion of the anterior SC: 0 = non-projecting anterosuperiorly; 1 = anterosuperiorly projecting.
#5	Shape of the posterior SC: 0 = vertically compressed; 1 = rounded; 2 = elongated superiorly.
#6	Shape of the lateral SC ampullary portion: 0 = flat or only slightly bent superiorly; 1 = markedly bent superiorly.
#7	Length of the CC: 0 = long; 1 = intermediate; 2 = short.

[a] See Figure 11 for an illustration of the character states.

Table 9

Character states coded for the estimated last common ancestors (LCAs) and for the fossil taxa included in the analysis.[a]

Species/LCAs	#1	#2	#3	#4	#5	#6	#7
Epipliopithecus vindobonensis	0	0	1	0	2	0	0
Aegyptopithecus zeuxis	0	0	2	0	2	0	0
Dolichocebus gaimanensis	0	0	2	0	2	0	0
Homunculus patagonicus	0	0	2	0	0, 2	0	0
Oreopithecus bambolii	1	1	0	1	1	0	2
Parapithecus grangeri	0	0	2	0	2	0	0
Crown anthropoid LCA	0	0	2	0	2	0	0
Crown platyrrhine LCA	0	0	2	0	2	0	0
Crown catarrhine LCA	0	0	1	0	1	0	1
Crown cercopithecoid LCA	0	0	1	0	1	0	1
Crown hominoid LCA	0	0	0	0	1	1	2
Crown hylobatid LCA	0	0	0	1	1	1	2
Crown hominid LCA	1	1	0	0	1	1	2

[a] See character definitions in Table 7 and SOM Table S2 for the coding of extant species.

Table 10

Measures of character congruence for the two main phylogenetic hypotheses (i.e., stem catarrhine vs. stem hominoid) discussed in this paper for *Epipliopithecus*. The higher the index, the more parsimonious the hypothesis.[a]

Metrics	Stem catarrhine (Fig. 3a)	Stem hominoid (Fig. 3b)
Tree length	22	24
CI	0.455	0.417
RI	0.826	0.797
RC	0.376	0.332

Abbreviations: CI = consistency index; RI = retention index; RC = rescaled consistency index.

[a] See also Figure 3 and SOM Table 2 for character descriptions.

Click here to access/download

e-Component

R4_SOM.pdf